Mon. Not. R. Astron. Soc. **000**, 1–20 (2005) Printed 6 June 2011 (MN LATEX style file v2.2)

Early magnetic B-type stars: X-ray emission and wind properties

L. M. Oskinova[1],⋆ H. Todt[1], R. Ignace[2], J. C. Brown[3], J. P. Cassinelli[4], W.-R. Hamann[1]
[1] *Institute for Physics and Astronomy, University of Potsdam, 14476 Potsdam, Germany*
[2] *Department of Physics and Astronomy, East Tennessee State University, Johnson City, TN 37614, USA*
[3] *School of Physics and Astronomy, University of Glasgow, Glasgow G12 8QQ, UK*
[4] *Department of Astronomy, University of Wisconsin-Madison, Madison, WI 53711, USA*

Accepted . Received ; in original form 21.02.2011 22:32

ABSTRACT

We present a comprehensive study of X-ray emission and wind properties of massive magnetic early B-type stars. Dedicated *XMM-Newton* observations were obtained for three early type B-type stars, ξ^1 CMa, V2052 Oph, and ζ Cas with recently discovered magnetic fields. We report the first detection of X-ray emission from V2052 Oph and ζ Cas. The latter is one the softest X-ray sources among early type stars, while the former is one of the X-ray faintest. The observations show that the X-ray spectra of our program stars are quite soft with the bulk of X-ray emitting material having a temperature of about 1 MK. We compile the complete sample of early B-type stars with detected magnetic fields to date and existing X-ray measurements, in order to study whether the X-ray emission can be used as a general proxy for stellar magnetism. We find that the X-ray properties of early massive B-type magnetic stars are diverse, and that hard and strong X-ray emission does not necessarily correlate with the presence of a magnetic field corroborating similar conclusions reached earlier for the classical chemically peculiar magnetic Bp-Ap stars.

We analyze the UV spectra of five non-supergiant B stars with magnetic fields (τ Sco, β Cep, ξ^1 CMa, V2052 Oph, and ζ Cas) by means of non-LTE iron-blanketed model atmospheres. The latter are calculated with the Potsdam Wolf-Rayet (PoWR) code, which treats the photosphere as well as the the wind, and also accounts for X-rays. With the exception of τ Sco, this is the first analysis of these stars by means of stellar wind models. Our models accurately fit the stellar photospheric spectra in the optical and the UV. The parameters of X-ray emission, temperature and flux are included in the model in accordance with observations. We confirm the earlier findings that the filling factors of X-ray emitting material are very high.

Our analysis reveals that the magnetic early type B stars studied here have weak winds with velocities not significantly exceeding $v_{\rm esc}$. The mass-loss rates inferred from the analysis of UV lines are significantly lower than predicted by hydrodynamically consistent models. We find that, although the X-rays strongly affect the ionisation structure of the wind, this effect is not sufficient in reducing the total radiative acceleration. When the X-rays are accounted for at the intensity and temperatures observed, there is still sufficient radiative acceleration to drive stronger mass-loss than we empirically infer from the UV spectral lines.

Key words: stars: massive – stars: magnetic field – stars: mass-loss – X-rays: stars – techniques: spectroscopic – stars: individual: ξ^1 CMa, τ Sco, β Cep, V2052 Oph, ζ Cas

1 INTRODUCTION

Magnetic fields in massive stars ($M_*{\gtrsim}8M_\odot$) have the potential to influence stellar formation and evolution (e.g. Ferrario et al. 2009). Although discoveries of massive star magnetism are increasing (Hubrig et al. 2011; Petit et al. 2011; Wade et al. 2011), our knowledge of their existence, origin and the role they play remains limited. The routine presence of magnetic fields in these stars is observationally neither established nor disproved, due to the lack hitherto of suitable diagnostic tools and observations of adequate quality (for a recent review see Donati & Landstreet 2009). The Zeeman effect, commonly used to measure magnetic fields in solar-type stars, is less useful in hot stars: the line broadening by macroscopic motions exceeds the Zeeman splitting, unless the magnetic field is extremely strong.

While direct measurements of magnetic field have been possible only for the closest and brightest stars, there has been indirect evidence for magnetic fields on massive stars. The wide range

⋆ E-mail: lida@astro.physik.uni-potsdam.de

of observational phenomena, such as UV wind-line periodic variability, cyclic variability in Hα and He II λ4686, and excess emission in UV-wind lines centered about the rest wavelength (e.g. Henrichs et al. 2005; Schnerr et al. 2008) are commonly explained by the influence that magnetic fields exert on stellar winds. For example, cyclical wind line variability is likely due to wind flow that is guided by a large scale, dipole-like magnetic field corotating with the star. In these cases the timescale of the variability is similar to the rotation period. Other indicators of magnetic fields may include chemical peculiarity, certain pulsation behavior, non-thermal radio emission, and anomalous X-ray emission.

In this paper we address the X-ray emission and wind properties of magnetic B-type stars. Our study includes stars earlier than B2 that have both confirmed magnetic fields and X-ray data. Thus, our sample includes only massive stars, with initial masses exceeding $\sim 8\,M_{\odot}$. We consider the B-type stars, where magnetic fields have been detected only recently as well as the earliest types of "classical" chemically peculiar Bp type stars. The latter have high incidence of strong magnetic fields (e.g. Bychkov et al. 2003). Much work has already been done to study the X-ray emission from chemically peculiar magnetic Bp and Ap stars. Using the results from X-ray surveys, correlations between the X-ray properties of these stars and their magnetism were investigated by Drake et al. (1994) and Leone (1994). Those works considered a broader range of spectral classes, not only B0-B2 stars as this work. The conclusion was reached that, despite some notable exceptions, there is little evidence that the X-ray emission from the Bp stars is different from other B-stars with similar spectral types. Czesla & Schmitt (2007) carried out *Chandra* high-angular resolution observations of a sample of late B-type and A-type stars with measured magnetic fields in the range from 0.2-17 kG. They showed that the existence of a magnetic field of kG strength on a late B-type or A-type star is not necessarily a prerequisite for finding X-ray emission among these stars.

The main focus of this work is on β Cephei-type variables and a slowly pulsating B-type star, where magnetic fields have been detected only recently. We performed dedicated observations with *XMM-Newton* for three magnetic B-stars: ξ^1 CMa, V2052 Oph, and ζ Cas. Two of them, V2052 Oph and ζ Cas are detected in X-rays for the first time. We also searched the X-ray archives to collect X-ray data for other magnetic early B-type stars. Thus, at the time of writing, we have assembled a complete sample of early-type magnetic B-stars for which X-ray observations are available. This sample will, undoubtedly, grow in future.

To infer stellar and wind parameters for the five stars in our sample we employ the non-LTE stellar atmosphere model PoWR (e.g. Hamann & Gräfener 2003).

Our sample of B-stars stars with directly measured magnetic fields is biased to non-supergiant stars. Our program stars allow us to explore the parameter space comprising different wind momenta, field strengths, and rotation periods with regard to the observed X-ray emission. We compare the properties of X-ray emission between our program stars and other B-type stars of similar spectral types, but without confirmed magnetic field. This allows investigation of whether the X-ray emission can serve as an indicator of the surface stellar magnetic field.

In the absence of a magnetic field, the mechanism that produces X-ray emission in early-type stars is thought to be the line-driven instability (LDI) that is an intrinsic property of stellar winds (Lucy & Solomon 1970). The LDI mechanism generates numerous shocks in a stellar wind, where plasma can be heated up to X-ray emitting temperatures (e.g. Feldmeier et al. 1997a,b).

In addition to the LDI mechanism, X-rays are thought to arise when magnetic fields are capable of governing the wind streams. Knowledge of the wind parameters, magnetic field topology and strength, together with X-ray observations provides a good basis to review critically the models of X-ray generation in massive magnetic stars.

Groote & Hunger (1982) proposed a scenario to explain observational phenomena associated with the B2Vp σ Ori E. Their model predicts the formation of a torus of matter around the star, formed by a weak stellar wind channeled along magnetic field lines. The torus is magnetically coupled to the star. Its co-rotation explains the observed photometric and spectroscopic variability. The X-ray emission is produced when the wind streams from opposing magnetic hemispheres collide leading to strong shock heating of the plasma. Townsend et al. (2007) further developed the Groote & Hunger (1982) scenario by using semi-analytical models of the rigidly rotating magnetosphere (RRM) in the limit of very strong ($\sim$few kG) magnetic fields. Their model predict very hard X-ray emission with temperatures up to 100 MK.

Babel & Montmerle (1997b) envisage a star with a dipole magnetic field that is sufficiently strong to confine the stellar wind. Collision between the wind components from the two hemispheres in the closed magnetosphere leads to a strong shock. The X-ray emission from the Ap-type star IQ Aur was explained in the framework of this "magnetically confined wind shock model" (MCWS), and the presence of a magnetic field in the O-type star θ^1 Ori C was postulated (Babel & Montmerle 1997a). The direct confirmation of the magnetic field in this star by Donati et al. (2002) proved that X-rays have diagnostic potential in selecting massive stars with surface magnetic fields. Numerical MHD simulations in the framework of the MCWS model were performed by ud-Doula & Owocki (2002). These simulations compare well with the X-ray observations of θ^1 Ori C (Gagné et al. 2005); however, the model has difficulties in describing the X-ray emission from other magnetic O-type stars (Nazé et al. 2010). In this paper we discuss the applicability of the MCWS model to the early-type magnetic B stars.

Cassinelli et al. (2002), Maheswaran (2003), Brown et al. (2008), and Maheswaran & Cassinelli (2009) studied the case of fast rotating magnetic massive stars with an increasing degree of model sophistication to address the formation of disks in classical Be-type stars. They showed that magnetic torquing and channeling of wind flow from intermediate latitudes on a B star could, for plausible field strengths, create a dense disk a few stellar radii in extent in which the velocity is azimuthal and of order the local Keplerian speed. Unlike all the other magnetically-guided wind scenarios mentioned, the disk model proposed by Brown et al. (2008) is in a steady state, wind inflow being offset by a very slow outflow across reconnecting field lines. Li et al. (2008) proposed a model, where the X-rays are produced by wind material that enters the shocks above and below the disk region. The model by Li et al. (2008) predicts a relation between the X-ray luminosity normalized to the stellar bolometric luminosity ($L_{\rm X}/L_{\rm bol}$) and the magnetic field strength in Be-type stars. Compared to the Be-type stars, the stars in our sample are slower rotators and have lower wind density.

The paper is organized as follows. Our program stars are introduced in Sect. 2. The new *XMM-Newton* observations are described in Sect. 3, and analyses of X-ray spectra presented in Sect. 4. The X-ray properties of early-type Bp stars are discussed in Sect. 5. Analysis of UV spectra for our program stars is presented in Sect. 6. We discuss our results in Section 7, with a summary of the main points given in Section 8.

Table 1. Magnetic early B-type stars with available X-ray observations

Name	HD	Sp	$B^{\rm a}$ G	$v \sin i$ km s^{-1}	$P_{\rm rot}$ d	Dipole	Obliquity$^{\rm b}$ β	Ref
τ Sco	149438	B0V	$\langle\sim 500\rangle$	5	41.033	no		*1*
β Cep-type and SPB-type stars								
ξ^1 CMa	46328	B0.7IV	5300 ± 1100	9 ± 2	2.18	yes	79.1	*2*
β Cep	205021	B2III	360 ± 40	27 ± 2	12.00089	yes	$85^\circ \pm 10^\circ$	*3, 4*
V2052 Oph	163472	B1V	250 ± 190	60 ± 4	3.63883	yes	$35^\circ \pm 18^\circ$	*5*
ζ Cas	3360	B2IV	335^{+120}_{-65}	17 ± 3	5.37045	yes	$77^\circ \pm 6^\circ$	*6*
Peculiar B stars								
NU Ori	37061	B0V(n)	$\sim$620	225 ± 50		yes		*7*
V1046 Ori	37017	B2V	$\langle\sim 1500\rangle$	$\lesssim$95	0.9	?	42°–59°	*8, 9, 13*
HR 3089	64740	B1.5Vp	$\langle 572 \pm 114\rangle$	160	1.33	?		*9, 13, 14*
LP Ori	36982	B2Vp	$\sim$1100	80 ± 20		yes		*7*
σ Ori E	37479	B2Vp	$\sim$10000	140 ± 10	1.191	yes	66°	*10*
HR 5907	142184	B2.5Ve	$\sim$20000	280	0.5083	yes(?)	4° (?)	*11, 12*

[a] for dipole field configuration, B is the polar field strength.
For τ Sco, HR 3089, and V1046 Ori, an approximate average field strength is shown in angle brackets
[b] β is the angle between the magnetic and rotational axes for the dipole field configuration
References: 1 Donati et al. (2006); Sota et al. (2011); *2* Hubrig et al. (2011); *3* Telting et al. (1997); *4* Donati et al. (2001); *5* Neiner et al. (2003b) *6* Neiner et al. (2003a); *7* Petit et al. (2008); *8* Bohlender et al. (1987); *9* Romanyuk & Kudryavtsev (2008); *10* Reiners et al. (2000); *11* Abt et al. (2002); *12* Grunhut et al. (2010); *13* Bychkov et al. (2003); *14* Borra & Landstreet (1979)

2 THE PROGRAM STARS

Our sample of early type magnetic B-stars with recently discovered magnetic fields includes the B0 type star τ Sco, the β Cephei type variables β Cep, ξ^1 CMa, and V2052 Oph, and the slow-pulsating B-type star (SPB) ζ Cas (see Table 1).

τ Sco is a well studied object, which has been observed in X-rays by all major X-ray missions. A complex magnetic field topology was discovered in τ Sco by Donati et al. (2006). τ Sco is a source of hard X-ray emission and displays narrow emission line profiles, suggesting nearly stationary plasma (Mewe et al. 2003). Recently, τ Sco was monitored throughout its rotational cycle by the *Suzaku* X-ray observatory. Contrary to expectations, rotational modulations of X-ray emission were not detected (Ignace et al. 2010). Magnetic fields were detected on two other stars, HD 66665 and HD 63425, that are spectroscopically similar to τ Sco (Petit et al. 2011). Although it remains to compare their X-ray characteristics to τ Sco, the new discoveries suggest that τ Sco may be a prototype for a wider class of stars.

β Cep, ξ^1 CMa and V2052 Oph are β Cephei type variables. β Cep-type stars have masses between 7 and 16 $M_\odot$ and are on the main-sequence or in an early post-MS evolutionary phase (corresponding to spectral type O9 to B3). Stars of this type display photometric and spectral variations caused by pulsations in low-order pressure and gravity modes of short-period (3–8 h) (Dziembowski & Pamiatnykh 1993).

A magnetic field in β Cep was detected by Henrichs et al. (2000). Based on the analysis of the *Rosat* measurements, Donati et al. (2001) suggested that the X-rays from β Cep can be explained within the framework of the MCWS model. This model predicts rotationally modulated, strong and hard X-ray emission originating at a few stellar radii from the surface close to the disk around the magnetic equator. However, data appear not to support these predictions. X-ray multiphase high-spectral resolution observations of β Cep by *XMM-Newton* and *Chandra* fail to show either rotational modulations or modulations on the time-scale of the stellar pulsations (Favata et al. 2009). The X-rays do not originate further out in the wind than 2-3 R_*, and the emission is quite soft with the bulk of X-ray emitting plasma at T≈3 MK, (Favata et al. 2009). The X-ray luminosity of β Cep is not atypical of stars with the same spectral type.

Hubrig et al. (2006) and Silvester et al. (2009) measured magnetic fields in a sample of eight β Cep-type stars. Both these studies agree in the lack of a definite detection of magnetic fields in the six β Cep-type stars, with typical longitudal field formal errors of few tens of G. The results of these investigations seems to indicate that the presence of a strong magnetic field is not a general intrinsic property of this spectral class.

Magnetic field measurements of ξ^1 CMa were reported in Hubrig et al. (2006) and confirmed by Silvester et al. (2009). Recently, (Hubrig et al. 2011) established the magnetic field configuration, and the rotational periods for a number of magnetic B-stars, among them ξ^1 CMa. It was shown that we see ξ^1 CMa nearly rotational pole-on.

ξ^1 CMa was previously observed in X-rays by *Einstein* and *Rosat*. Cassinelli et al. (1994) presented a *Rosat* PSPC spectrum of this star. They reported a temperature of 3.7 MK and an emission measure EM$\sim 10^{54}$ cm^{-3}, and pointed out that ξ^1 CMa has the highest X-ray luminosity and the hardest spectrum among the β Cep-type stars in their sample.

The detection of a magnetic field in V2052 Oph was reported by Neiner et al. (2003b). The polar magnetic field was determined assuming that the star is an oblique rotator. Neiner et al. (2003b) note that V2052 Oph is very similar to β Cep. They suggested that based on β Cep, the wind of V2052 Oph should be confined and form a disk-like structure. Prior to our observations, there was no positive detection of X-ray emission from V2052 Oph, with the *Rosat All Sky Survey* (RASS) yielding only an upper limit to its X-ray luminosity.

The slow-pulsating B stars are slightly less luminous and cooler than the β Cep-type stars. These stars show multi-periodic brightness and color variations on a time-scale of 0.8 d–3 d.

Table 2. *XMM-Newton* observations of three magnetic early B-type stars

Star	MJD	useful exposure [ksec]	PN count-rate[a] [s^{-1}]
ξ^1 CMa	55046.4576	6.9	0.61 ± 0.01
V2052 Oph	55077.0906	9.2	0.003 ± 0.001
ζ Cas	55046.4576	12.3	0.040 ± 0.002

[a] in the 0.3-7.0 keV band; background subtracted

Neiner et al. (2003a) reported the discovery of a magnetic field on the SPB star ζ Cas. Hubrig et al. (2006) and Silvester et al. (2009) searched for magnetic fields in a large sample of SPB stars; however, the results of their measurements agree only partially – both studies detect a magnetic field on 16 Peg (B3V) (Silvester et al. (2009) report a marginal detection). 16 Peg is not yet detected in X-rays. Prior to our observations, there were no positive detection of X-ray emission from ζ Cas either, with the RASS yielding an upper limit to its X-ray luminosity. Neiner et al. (2003a) analyzed the magnetic field configuration of ζ Cas and concluded that the star is an oblique magnetic dipole. However, they argued that there is no evidence for a disk around this star, based on the lack of an IR excess.

3 OBSERVATIONS

We obtained dedicated *XMM-Newton* observations of ξ^1 CMa, ζ Cas, and V2052 Oph. All three (MOS1, MOS2, and PN) European Photon Imaging Cameras (EPICs) were operated in the standard, full-frame mode and a thick UV filter (Turner et al. 2001; Strüder et al. 2001). The log of observations is shown in Table 2. The data were analyzed using the software SAS 9.0.0. Each of the stars in our sample was detected by the standard source detection software. The exposure times and EPIC PN count rates for our program stars are given in Table 2. The spectra and light-curves were extracted using standard procedures. The spectra of all sources were extracted from regions with diameter $\approx 15''$. The background areas were chosen in nearby areas free of X-ray sources. The EPIC PN spectra of ξ^1 CMa were corrected for "out-of-time events".

4 X-RAY SPECTRA AND THEIR FITTING

To analyze the spectra we used the standard spectral fitting software XSPEC (Arnaud 1996). The reference abundances were set to solar values according to Asplund et al. (2009). The number of counts per bin in the spectra of ζ Cas and V2052 Oph is small, therefore we used Cash-statistic (Cash 1979) to fit their spectra, while the ξ^1 CMa spectra were fitted using the χ^2-statistics. Using the neutral hydrogen column density as a fitting parameter does not yield a sensible constraint on its value. Therefore, $N_{\rm H}$ was fixed at its interstellar value as found from the analysis of optical and UV spectra (see Section 6) for all our program stars.

The standard model *vapec*, which assumes that the plasma is in collisional ionization equilibrium (CIE), was used to model the observed X-ray spectra of our program stars. CIE models require that several equilibria exist in the stellar wind namely that the electrons and ions are both thermalized and have equilibrated so as to have $T_{\rm e} = T_{\rm i}$ and that ionization and recombination rates are balanced. The thermalization processes is controlled by Coulomb collisions or even faster plasma effects. However, cooling of the plasma can be faster than the overall recombination time due to of some ions with important cooling lines. Sutherland & Dopita (1993) provide a comparison of the collisional equilibrium timescale and the cooling timescale for carbon and iron ions. From their Fig. 15, at temperatures above $\gtrsim$1 MK, the cooling time is $\tau_{\rm cool} = 1.5nkT/n_{\rm e}n_{\rm i}\Lambda(T) > 5\times10^8/n_{\rm e})$ hr, and the collisional equilibrium time for C VI is $\tau_{\rm recomb} = \alpha^{-1}_{\rm recomb} \cdot n_{\rm e}^{-1} < 1.5 \times 10^8 (1\,{\rm cm}^{-3}/n_{\rm e})$ hr, where $n_{\rm e}$ and $n_{\rm i}$ are electron and ion number densities respectively in cm^{-3}, $\Lambda(T)$ is the cooling function, and $\alpha_{\rm recomb}$ is the recombination coefficient (see Sutherland & Dopita (1993) for details). Hence, at the temperatures where the maximum of emission measure is determined from the analysis of X-ray spectra (see Table 3), the cooling of the plasma is slower than the recombination time-scale, and the conditions for the establishing the CIE seem to be fulfilled.

Using ξ^1 CMa as an example, we deduce from our wind models (see Section 6) that at 1 R_* distance from the photosphere, the electron density in the wind is $\sim 10^7$ cm^{-3}. The cooling time of a 1 MK plasma is ≈ 50 hr, while the collisional equilibrium time for C VI is ≈ 15 hr. Note that this is long compared to the pulsational time-scale of β Cep-type variables, e.g. the pulsational period of ξ^1 CMa is 5.03 hr (Stankov & Handler 2005).

The mean free path for a Coulomb collision $l_{\rm mfp} \approx 9.4 \times 10^7 T^2 n_8^{-1}$ cm, where T is in the units of MK, and n_8 is in the units of 10^8 cm^{-3}. Using parameters for ξ^1 CMa close to the stellar surface, the value of $l_{\rm mfp}$ is only 100 cm. Therefore, we believe that the use of CIE models to describe the X-ray spectra of our program stars is justified.

The chemical abundances of our program stars deviate from the solar, which is most likely a consequence of the surface magnetic field. Peculiar abundances are often found in magnetic stars, and is commonly explained by diffusion processes which allow heavier elements to sink in the atmosphere under the influence of gravity, while lighter elements are lifted to the surface by radiation pressure. The summary of the relevant publications with analyses of abundances in our program stars can be found in Neiner et al. (2003b), Neiner et al. (2003a) and Morel et al. (2008). In summary, these studies agree that the magnetic stars show an overabundance of nitrogen, and sometimes helium. The quality of the X-ray spectra are not sufficient to constrain abundances. Therefore, for each star we have used the abundances determined by Morel et al. (2008).

ξ^1 CMa The observed EPIC spectra of ξ^1 CMa and the fitted model are shown in Fig. 1. The abundances were set to solar values, except C/C$_\odot$=0.56, N/N$_\odot$=1.48, and O/O$_\odot$=0.79, as found by Morel et al. (2008). We initially attempted to fit the spectra using two temperature models similar to Favata et al. (2009) for modeling the β Cep X-ray spectrum. However, we found that adding a softer model component with $kT \approx 0.1$ keV significantly improved the quality of the fit. Parameters of the best-fit model are shown in Table 3. We also attempted to fit the ξ^1 CMa spectrum assuming a higher temperature component. By analogy with the τ Sco spectral models (Mewe et al. 2003), a spectral model component with $kT_4 = 1.7$ keV was assumed. However, the emission measure of this hot component cannot be constrained. As a next step, we investigated whether the ξ^1 CMa spectrum can be fitted with non-equilibrium ionization models. Using the *nei* model available in XSPEC, we failed to find a suitable set of model parameters to reproduce the observed spectrum.

V2052 Oph Our *XMM-Newton* observation detected the X-ray emission from V2052 Oph for the first time. The source has a very

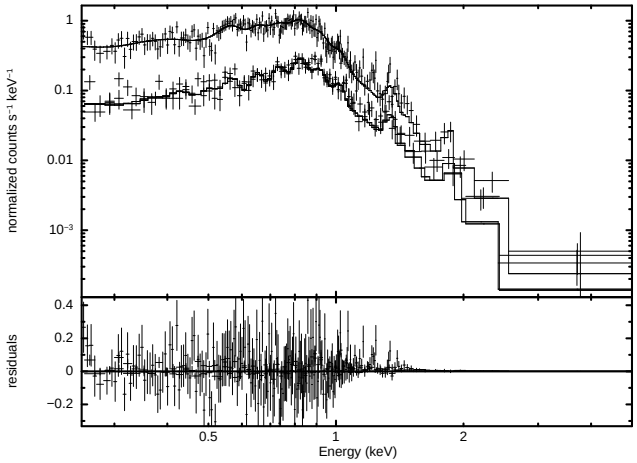

Figure 1. *XMM-Newton* PN (upper curve), and MOS1 and MOS2 (lower curves) spectra of ξ^1 CMa with the best fit three-temperature model (solid lines). The model parameters are shown in Table 3.

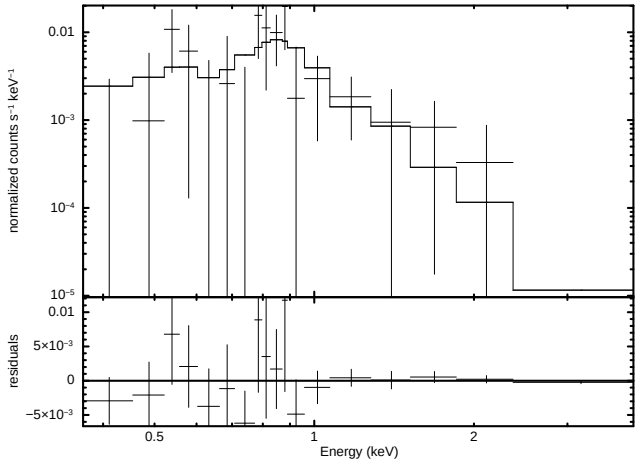

Figure 2. *XMM-Newton* EPIC-PN spectrum of V2052 Oph and the best fit two-temperature model. The model parameters are shown in Table 3.

low count rate (see Table 2); in total only about 60 source counts were collected. At a distance of $d = 417$ pc, the X-ray luminosity of V2052 Oph is only $L_{\rm X} \approx 3 \times 10^{29}$ erg s^{-1}, making it one of the least X-ray luminous early type B-stars in the sky. To model the observed low S/N spectrum, we fixed the neutral hydrogen column density at its interstellar value. The PN spectrum of V2052 Oph can be well described using a two temperature plasma model see Table 3). The abundances C/C$_\odot$=0.6, N/N$_\odot$=1.4, and O/O$_\odot$=0.5 were used as found by Morel et al. (2008). The temperature and the emission measure of soft component are only poorly constrained but the presence of a soft component is required to reproduce the observed hardness ratio. There are no indications of a harder component being present in the spectrum of V2052 Oph.

Pausing to consider the X-ray spectral analyses of the β Cep-type stars (β Cep, ξ^1 CMa and V2052 Oph), it emerges that the spectral temperatures are similar among these stars. We define the mean spectral temperature $\langle kT \rangle$ as the emission measure weighted average temperature, with

$$\langle kT \rangle \equiv \sum_i kT_i \cdot {\rm EM}_i / \sum_i {\rm EM}_i. \quad (1)$$

Then, the mean spectral temperature for all magnetic β Cep-type stars is the same at ≈3.5 MK (see Table 3). However, we find a large difference in X-ray luminosities for the β Cep stars, with ξ^1 CMa being 4 times more X-ray luminous than β Cep and 50 times more X-ray luminous than V2052 Oph (see Table 1).

ζ Cas Our *XMM-Newton* observations of ζ Cas are the first X-ray observations to yield a spectrum of a magnetic SPB-star. Visual inspection of EPIC *XMM-Newton* images already reveals that ζ Cas is a very soft X-ray source. This expectation is confirmed by the X-ray spectral fits. The EPIC spectra of ζ Cas and the best fit 2T CIE model are shown in Fig. 3. A solar composition was assumed, except for C/C$_\odot$=0.5, N/N$_\odot$=1.4, and O/O$_\odot$=0.5 (Morel et al. 2008). Parameters of the model are shown in Table 3. The maximum temperature inferred from the spectral analysis is ≈4 MK, and there are no indications of a harder spectral component. The emission measure is dominated by the 1 MK plasma; the hotter, 4 MK component constitutes less than 20% of the total emission measure. ζ Cas has the softest X-ray spectrum among all hot stars where magnetic field

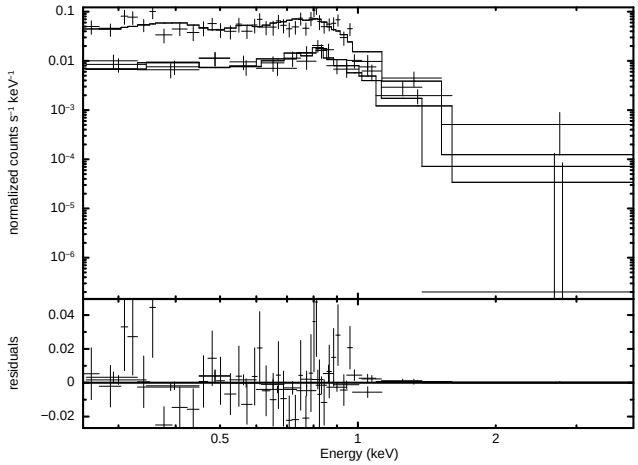

Figure 3. *XMM-Newton* EPIC PN (upper), and MOS1 and MOS2 (lower) spectra of ζ Cas and the best fit two-temperature model. The model parameters are shown in Table 3.

have been detected. The mean X-ray spectral temperature of ζ Cas is about 1 MK (see Table 3).

5 X-RAY PROPERTIES OF CLASSICAL PECULIAR MAGNETIC EARLY-TYPE B STARS

In this section we briefly consider the X-ray properties of chemically peculiar Bp-stars, addressing only stars with early spectral types. The classical chemically peculiar Bp-Ap stars have a high incidence of strong surface magnetic fields. The observed temporal variations of longitudal magnetic fields are usually compatible with dipole or low-order multipole fields inclined to the rotation axis (Donati & Landstreet 2009). The strong magnetic fields strongly influence weak stellar winds, making the Bp stars excellent test cases for models of X-ray production in magnetic early-type stars.

There has been earlier work seeking to establish the X-ray properties of chemically peculiar stars. Drake et al. (1994) searched the RASS database at the positions of about 100 magnetic Bp-Ap stars. They detected 10 X-ray sources and argued that in four cases the X-ray emission presumably arises from an early-type star with a radiatively driven wind. The X-ray luminosities were found to

Table 3. The spectral parameters derived from the *XMM-Newton* EPIC observations of our program stars assuming the multi-temperature CIE plasma models (*vapec*) corrected for the interstellar absorption (*tbabs*). The values which have no error have been frozen during the fitting process. The corresponding spectral fits are shown in Figs. 1,3,2. For comparison, the spectral parameters inferred from modeling *XMM-Newton* data of β Cep and *Suzaku* spectra of τ Sco are also shown.

Star	ξ^1 CMa	ζ Cas	V2052 Oph	β Cep[a]	τ Sco[b]
$N_{\rm H}^{\rm c}$ [10^{20} cm^{-2}]	1.4	3	15	2.5 ± 0.1	3
kT_1 [keV]	0.12 ± 0.01	0.08 ± 0.02	0.14 ± 0.12	0.24 ± 0.01	0.11 ± 0.01
EM$_1$ [10^{53}cm^{-6}]	22.48 ± 5.64	1.29 ± 1.05	0.006 ± 0.025	11 ± 2	17.0 ± 2.61
kT_2 [keV]	0.32 ± 0.01	0.31 ± 0.02			0.34 ± 0.01
EM$_2$ [10^{53}cm^{-3}]	19.3 ± 3.36	0.27 ± 0.07			10.4 ± 0.51
kT_3 [keV]	0.68 ± 0.05		0.65 ± 0.11	0.69 ± 0.03	0.71 ± 0.10
EM$_3$ [10^{53} cm^{-6}]	6.41 ± 2.57		0.003 ± 0.002	1.3 ± 0.3	7.2 ± 0.3
kT_4 [keV]					1.52 ± 0.06
EM$_4$ [10^{53} cm^{-6}]					5.2 ± 0.3
$\langle kT \rangle \equiv \sum_i kT_i \cdot {\rm EM}_i / \sum_i {\rm EM}_i$ [keV]	0.3	0.1	0.3	0.3	0.5
Flux[d] [10^{-12} erg cm^{-2} s^{-1}]	1.1	0.093	0.006	1.0	16.4

[a] the values are adopted from Favata et al. (2009)

[b] the values are adopted from Ignace et al. (2010)

[c] correspond to the ISM hydrogen column density for all stars

[d] in the 0.3-7.0 keV band, except of τ Sco in the 0.3-10.0 keV band, absorbed;

be in general agreement with the canonical values of X-ray emission from massive stars $L_{\rm X} \approx 10^{-7}\, L_{\rm bol}$. E.g., the B1.5Vp star HR 3089 has $\log L_{\rm X}/L_{\rm bol} \approx -7.2$.

To include newer data, we selected Bp stars with spectral types earlier than B2 from *The Catalog of Peculiar Magnetic Stars* (Romanyuk & Kudryavtsev 2008). This sample was augmented by two more magnetic Bp-type stars reported by Petit et al. (2008) and the magnetic Be star HR 5907 recently reported by the MiMeS collaboration (Grunhut et al. 2010). As a next step we searched the available X-ray catalogs. Our search revealed that σ Ori E, LP Ori, NU Ori, and V1046 Ori, HR 5907 have positive X-ray detections.

σ Ori E is the prototypical oblique fast magnetic rotator. Its X-ray emission is quite hard: the EM of 10 MK plasma is as large as the EM of the cooler plasma with T$\approx$ 3 MK (Sanz-Forcada et al. 2004). The mean spectral temperature of σ Ori E (in quiescence) is 0.66 keV or 7.6 MK. We estimate the bolometric luminosity of σ Ori E, $\log L_{\rm bol}/L_{\odot} = 3.8$, based on its spectral type and UBV colours and assuming a distance of 640 pc (Hunger et al. 1989). The average (quiescent+flare) X-ray luminosity in 0.1-2.4 keV band at 640 pc is $L_{\rm X} \approx 8 \times 10^{31}$ erg s^{-1}, the quiescent X-ray luminosity is factor of 5 lower than in the peak (Sanz-Forcada et al. 2004). The star is X-ray luminous: its ratio of X-ray to bolometric luminosities $L_{\rm X}/L_{\rm bol}$ is nearly two orders of magnitude higher than normally found in B-type stars (see Table 4). An extremely rare event in the history of X-ray observations of massive hot stars – an X-ray flare – has been observed from σ Ori E (Groote & Schmitt 2004; Sanz-Forcada et al. 2004) that may be understood as a result of centrifugal breakout of the torus (Mullan 2009). These X-ray properties of σ Ori E seems to confirm the expectations of the RRM model (Townsend et al. 2007).

Given the general nature of these models, one would naturally expect that these results could be applied to other BV stars with strong magnetic fields. This however, seems not to be the case.

The young star LP Ori is similar to σ Ori E in many respects: it has a similar age, spectral type, and a kG strong magnetic field. It is also a source of hard X-ray emission (Getman et al. 2005). However, the X-ray luminosity of LP Ori is significantly lower than the X-ray luminosity of σ Ori E. In fact, the X-ray luminosity of LP Ori is nearly the lowest one among all magnetic early B-stars (see Table 4). The models predicts modulations of the X-ray luminosity due to the occultation of X-ray emitting site by the opaque torus. These modulations are thought to occur on a time-scale comparable to the rotational period of the star. LP Ori was observed by *Chandra* for ≈8.8 d (Getman et al. 2005). This long exposure time suggests that the observed X-ray flux is somewhat averaged over the rotational period, and the star is indeed intrinsically faint in X-rays.

X-ray observations of σ Ori E and LP Ori seemingly suggest that the strong magnetism may account for the hardness of the X-ray emission. However, the Bp stars V1046 Ori and NU Ori provide counter examples.

Similar to σ Ori E, V1046 Ori has a kG magnetic field. It also is an oblique magnetic rotator, whose obliquity and rotational period are similar to that of σ Ori E. The star was serendipitously observed by *XMM-Newton*. No X-ray spectra are available, but hardness ratios are provided in *The Second XMM-Newton Serendipitous Source Catalog or 2XMMi-DR3* and in Nazé (2009). We have compared these hardness ratios with those of τ Sco reported in the same catalog. V1046 Ori is a softer X-ray source compared to τ Sco, and its X-ray luminosity is relatively low (see Table 4). We estimate its bolometric luminosity based on UBV colors and spectral type.

The magnetic field on NU Ori is only about ∼0.5 kG and is weaker than the fields of the other Bp stars in our sample. Petit et al. (2008, and references therein) comment on NU Ori being a triple system, containing a massive B0.5V primary, along with a low mass spectroscopic companion and a visual companion. NU Ori was recently analyzed by Simón-Díaz et al. (2011), who obtained $\log L_{\rm bol}/L_{\odot} = 4.4$. NU Ori was observed by *Chandra* simultaneously with LP Ori (Getman et al. 2005). Surprisingly, that analysis indicates that the X-ray luminosity of NU Ori is a factor of 30 higher than for LP Ori, yet the former has a considerably softer emission as compared to the latter.

HR 5907 has very strong magnetic field (Grunhut et al. 2010).

Table 4. X-ray luminosities of magnetic early B-type stars

Name	d	$L_{\rm X}$	$\log(L_{\rm X}/L_{\rm bol})$
	pc	10^{30} erg s^{-1}	
τ Sco	150	40	-6.4
Magnetic β Cep-type and SPB-type stars			
ξ^1 CMa	420	30	-6.6
β Cep	200	6.4	-7.0
V2052 Oph	400	0.3	-8.0
ζ Cas	180	0.5	-7.5
Other magnetic early-type B stars			
NU Ori	400	1.0	-8
V1046 Ori[a]	380	0.1	-8.0
σ Ori E[b]	640	80	-5.6
HR 3089[c]	300	2	-7.2
LP Ori	470	0.02	-8.5
HR 5907	120	0.4	-7.4

Distances are from van Leeuwen (2007) except of LP Ori, σ Ori E, HR 3089;
[a] the distance between the X-ray source;
2XMM J053522.0-042938 and the position of V1046 Ori is $3''$;
[b] $L_{\rm X}$ (quiescent+flare) in 0.1-2.4 keV band from Sanz-Forcada et al. (2004) ;
[c] $L_{\rm X}$ in 0.1-2.4 keV band from Drake et al. (1994);

Assuming a dipole, the field strength at the pole is ≈ 20 kG. The star is a fast rotator with $v \sin i \approx 280\,{\rm km\,s^{-1}}$ (Abt et al. 2002). Yudin (2001) detect intrinsic polarization on the level 0.17% in V band and consider this star as a classical Be star with a disk. The star was observed by *Rosat* PSPC for ≈ 4.8 ks. It is detected with a flux $\approx 2 \times 10^{-13}$ erg cm^{-2} s^{-1} corresponding to rather low X-ray luminosity (see Table 4). We fit the low signal-to-noise *Rosat* PSPC spectra and find that HR 5907 has a relatively hard spectrum characterized by a temperature above 1 keV.

The rigidly rotating magnetosphere scenario makes robust predictions of strong, variable, and hard X-ray emission. It appears that in five out of the six early-type magnetized B stars under discussion, these predictions are not fulfilled. Considering just our small sample of early-type B stars with kG strong magnetic fields, we must conclude that the new measurements confirm earlier results on the X-ray emission from Bp-Ap stars. The properties of their X-ray emission are quite diverse, with majority of the stars emitting X-rays on the level typical for the general sample of B-stars (e.g Drake et al. 1994).

Placed in the context of this earlier work, our results corroborate the basic conclusion that while strong and hard X-ray emission is sufficient to suggest a star may be magnetic, it is not a required property of magnetic stars.

6 STELLAR WINDS

The strong UV radiation of B-type stars drives their stellar winds. The parameters of stellar winds are commonly inferred from the analyses of optical and UV spectral lines by means of stellar atmosphere models. While the B-type giants and supergiants have often been analyzed, the winds of BIV and BV type stars yet remained relatively unexplored. Prinja (1989) used profile fits to model spectral lines of C IV, Si IV, and Si III in high-resolution spectra of B stars obtained with the International Ultraviolet Explorer (IUE), and produced a homogeneous set of wind-velocity and column-density measurements for 40 non-emission, non-supergiant B stars. It was concluded that the presence of C IV resonance doublet in their UV spectra must be due to the effect of X-rays on wind ionization. This effect is often referred to as "superionization". Prinja (1989) did not find any asymmetry in the Si IV lines which would be typical if the stellar wind was strong. Estimates of column densities revealed that the mass-loss rates in non-supergiant B stars are significantly lower than in O and Be stars. From fitting the UV resonance lines of C IV and Si IV, it was found that the products of mass-loss rate and ionization fraction, $\dot{M}q$, are $\ll 10^{-10}\,M_\odot\,{\rm yr}^{-1}$. Regarding the wind velocities, it was shown that the winds of "normal" non-supergiant stars are slow compared to those of the Be stars. The maximum observed wind velocities do not generally exceed the stellar escape velocity.

Table 5. UV observations of program stars used in the analysis

object	data set	date
ζ Cas	SWP 51309	04/07/1994
ξ^1 CMa	SWP 03574	12/12/1978
τ Sco	SWP 55997	23/09/1995
V 2052 Oph	SWP 50431	31/03/1994
β Cep	SWP40477	28/12/1990

In this paper we analyze the UV spectra of our sample magnetic stars by means of a stellar atmosphere code. Stellar spectroscopy codes used to analyze massive stars are based on spherically symmetric or plane-parallel geometries, despite of the clear observational evidence that massive star winds can depart from spherical symmetry (e.g. Kaper et al. 1997; Hamann et al. 2001). It is very probable that magnetic fields affect the wind geometry. However, at present 3D modeling of stellar winds that would allow quantitative spectroscopic analysis is beyond reach. Our approach allows to conduct a multiwavelength X-ray and UV/optical spectral analysis. The obtained wind parameters of our sample stars can be compared to other massive stars in the general framework of massive star wind quantitative spectroscopy.

6.1 Model description: PoWR stellar atmosphere

In this work we analyze the spectra of magnetic B stars by means of stellar atmosphere models that account for the presence of X-rays. We use the Potsdam Wolf-Rayet (PoWR) model atmosphere code (Hamann & Gräfener 2003, 2004). The PoWR code has been used extensively to analyze not only massive stars with strong stellar winds (e.g. Liermann et al. 2010), but also low-mass central stars of planetary nebulae, and extreme helium stars (Hamann 2010; Todt et al. 2010). The PoWR code solves the non-LTE radiative transfer in a spherically expanding atmosphere simultaneously with the statistical equilibrium equations and accounts at the same time for energy conservation. Complex model atoms with hundreds of levels and thousands of transitions are taken into account. The computations for the present paper include complex atomic models for hydrogen, helium, carbon, oxygen, nitrogen, and silicon. Iron and iron-group elements with millions of lines are included in the PoWR code through the concept of superlevels (Gräfener et al. 2002). The extensive inclusion of the iron group elements is important not only because of their blanketing effect on the atmospheric structure, but also because the diagnostic wind lines in the UV (e.g. the C IV and Si IV resonance lines) are heavily blended with the "iron forest".

The PoWR models can take account of stellar-wind clumping in the standard volume-filling factor 'microclumping' approach (e.g. Hamann & Koesterke 1998), or even, with an approximate correction for wind clumps of arbitrary optical depth ("macro-

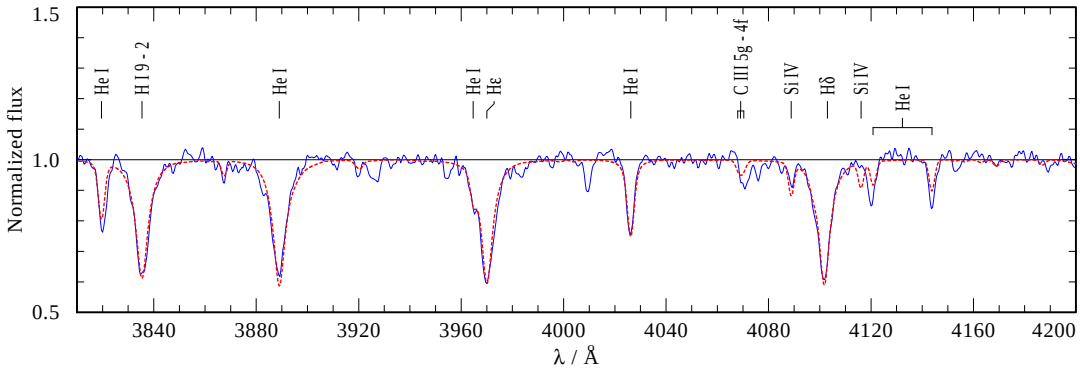

Figure 4. Optical CTIO spectrum of ξ^1 CMa obtained on 1988/11/02 (Walborn & Fitzpatrick 1990) (blue line) vs. a PoWR model spectrum (red line) using stellar parameters of ξ^1 CMa as shown in Table 6. The model spectrum is convolved with a 2.5 Å Gaussian to match the spectral resolution of the "2D-Frutti" spectrograph at CTIO.

clumping", Oskinova et al. 2007). However, since the wind signatures are quite weak for all stars of our sample, and since there is no way to estimate the degree of clumping, we apply here only smooth-wind models. Note that microclumping does not directly influence the resonance line profile shapes via radiative transfer effects, but can indirectly affect the lines by virtue of modifying the ionization stratification.

The X-ray emission and its effects on the ionization structure of the wind is included in the PoWR atmosphere models according to the recipe of Baum et al. (1992). We assume an optically thin, hot plasma component distributed within the "cool" stellar wind. The uniform value of the so-called Emission Measure 'filling factor' , $X_{\rm fill} = EM_{\rm hot}/EM_{\rm cool}$ (really a density squared weighted volume ratio), is adjusted such that the emergent X-ray luminosity agrees with the observations. The X-ray emissivity is restricted to the fast-wind domain, for which we assume a minimum radius of 1.1 R_*. The absorption of the X-ray radiation by the "cool" stellar wind is taken into account, as well as its effect on the ionization stratification by the Auger process.

The lower boundary of the model atmosphere is set at a Rosseland depth of 20, meaning that the (nearly) static photosphere is included in the computations. The velocity field consists of two parts. In the photospheric part of the atmosphere, a hydrostatic density stratification is assumed, while for the wind the usual "β-law" prescription is adopted, in our case with an exponent $\beta = 1$. We also tested the so-called double-β law (Hillier & Miller 1999), but without substantial improvement of the fit quality.

Each stellar atmosphere model is defined by the effective temperature, surface gravity, luminosity, mass-loss rate, wind terminal velocity v_∞, and chemical composition. The gravity determines the density structure of the stellar atmosphere below and close to the sonic point. From the pressure-broadened profiles of photospheric lines, the spectroscopic analysis allows derivation of the gravity and thus the stellar mass. For our sample of B stars, we confirm a discrepancy between the spectroscopic and evolutionary mass, the former being lower than the latter (see Weidner & Vink (2010) and references therein).

Dedicated analyses of the photospheric spectra of our program stars have been performed by Neiner et al. (2003b), Neiner et al. (2003a) and Morel et al. (2008). Using their abundances, $T_{\rm eff}$, and $\log g$ we find that our model reproduces photospheric spectra very well, as demonstrated by the example shown in Fig. 4. Therefore, to speed up the analysis, we adopt the literature values of $T_{\rm eff}$, and $\log g$. The effects of rotation with values $v \sin i$ from Table 1 are also included in the models.

All stars in our sample have measured parallaxes. Hence we can scale synthetic spectral energy distributions (SED) to that distance and fit to the observations, covering the whole wavelength range from the UV to IR. Furthermore, the model spectra are corrected for interstellar extinction. Dust extinction is taken into account using the reddening law of Cardelli et al. (1989). An example of a SED fit is shown in Fig. 5. The figure also shows the model continuum without lines, illustrating how the "forest" of iron lines forms a pseudo-continuum in the UV that is well reproduced by our model.

With $\log g$, $T_{\rm eff}$, and $L_{\rm bol}$ being fixed, we compare the synthetic and observed lines varying the wind parameters $\dot{M}$ and v_∞ in order to achieve the best fit. The usual indicators of mass loss used in B supergiants and Be stars, as well as in O-type stars, are Hα together with the UV resonance lines. However, in our sample of non-supergiant stars the Hα line is entirely photospheric[1]. Therefore, our wind diagnostic can only be based on the UV resonance lines. High resolution IUE spectra were retrieved from the archive for all stars of our sample. For some of them, multiple IUE observations are available (see e.g. the IUE time series for β Cep and ξ^1 CMa in Schnerr et al. 2008). In those cases we selected the observation of best quality (cf. Table 5).

6.2 τ Sco

τ Sco is a well studied object that has remained one of the primary targets in stellar UV and X-ray astronomy from their early days (e.g. Rogerson & Upson 1977; Macfarlane & Cassinelli 1989). It was one of the first stars whose UV spectrum was analyzed by means of atmosphere models based on co-moving radiative transfer techniques by Hamann (1981), who obtained a mass-loss rate $\log \dot{M} = -8.9 \pm 0.5$ from the analysis of UV lines. It was also shown that O VI and N V lines cannot be reproduced by the cool wind models. Cassinelli & Olson (1979) explained the presence of O VI and N V as arising from Auger ionization by X-rays.

We re-analyzed the wind properties of τ Sco using the PoWR model. The abundances as presented in Hubrig et al. (2008) were

[1] β Cep shows Hα emission episodes. However, Schnerr et al. (2006) found that the Hα emission is not related to the primary in β Cep, but is due to its 3.4 mag fainter companion that is a classical Be star.

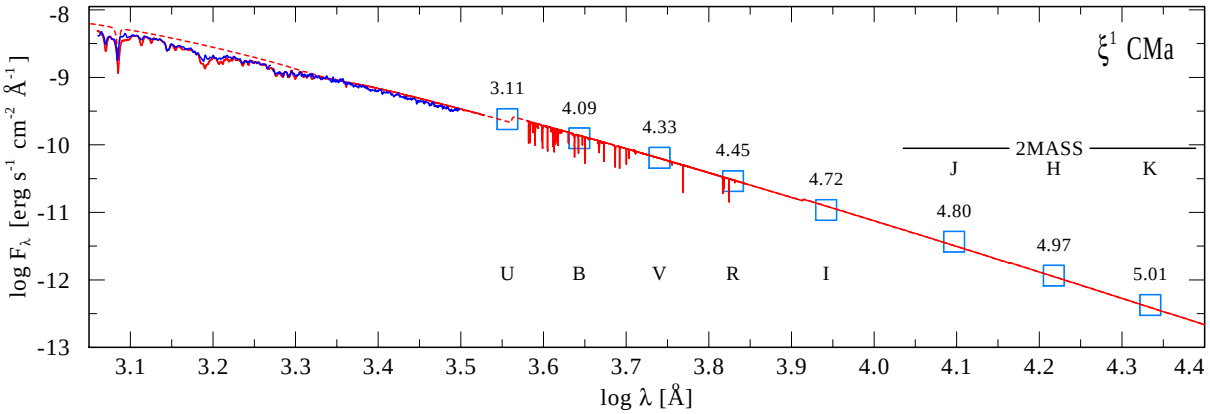

Figure 5. Spectral energy distribution for ξ^1 CMa. Observed IUE spectra are shown as thin blue lines. Blue boxes indicate observed photometry (labels: magnitudes) taken from the 2MASS catalogue (Skrutskie et al. 2006) and from Morel & Magnenat (1978). The synthetic spectrum (red line) is calculated using parameters given in Table 6. The model flux is reddened with $E_{\mathrm{B-V}} = 0.04$ and corrected for interstellar Lyman line absorption. The model continuum without lines (red dotted) is also shown to demonstrate how the iron group lines form a pseudo-continuum in the UV.

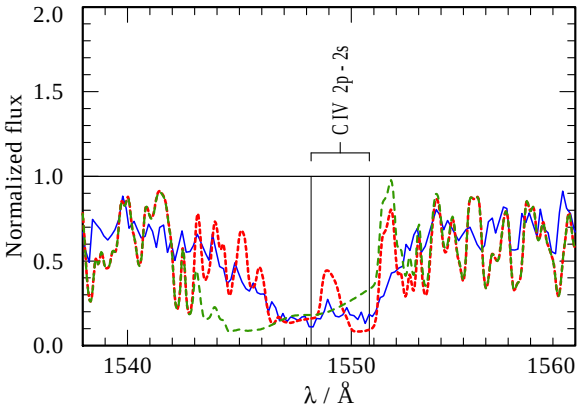

Figure 6. τ Sco: The effect of ionization by X-rays on C IV $\lambda\lambda$1548.2, 1550.8 Å doublet. Detail of the UV spectrum observed with IUE (blue thin line) vs. PoWR models: without X-rays (green dotted line) and with X-rays (red thick line). The model parameters: $\log(\dot{M}) = -9.3$, $v_\infty = 1000$ km/s. This figure shows that C IV is efficiently destroyed by X-rays in the outer parts of the atmosphere. Without accounting for the ionization by X-rays, the mass-loss rate would be underestimated.

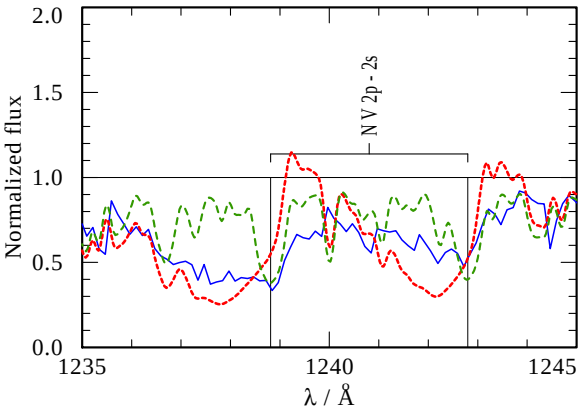

Figure 7. τ Sco: Same as in Fig. 6 but centered on the N V doublet.

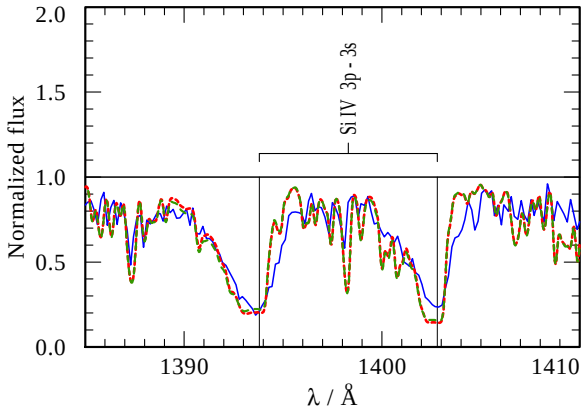

Figure 8. τ Sco: Same as in Figs. 6 and 7 but centered on the Si IV doublet. The model parameters: $\log(\dot{M}) = -8.6$, $v_\infty = 1000$ km/s. Note that even without X-rays, most silicon is already ionized to Si V in the outer parts of the atmosphere, therefore the Si IV doublet is insensitive to X-rays.

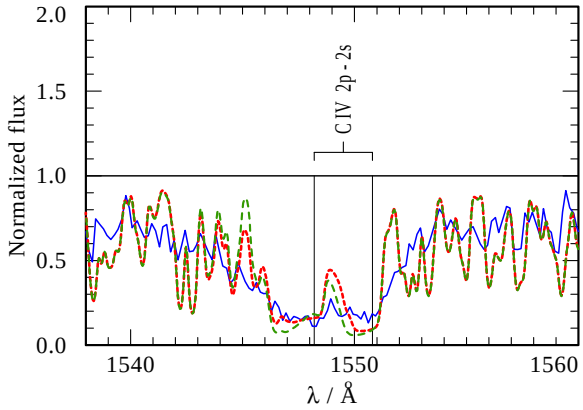

Figure 9. τ Sco: Determination of the wind velocity from modeling the C IV line. Detail of the UV spectrum observed with IUE (blue thin line) vs. PoWR models with $v_\infty = 500\,\mathrm{km\,s^{-1}}$ (green dotted line) and $v_\infty = 1000\,\mathrm{km\,s^{-1}}$ (red dotted line). The derived mass-loss rate is $\log(\dot{M}) = -9.3$. The blue absorption wing of the C IV line is better matched by the model with higher v_∞. Both models include ionization due to X-rays with parameters as listed in Table 1.

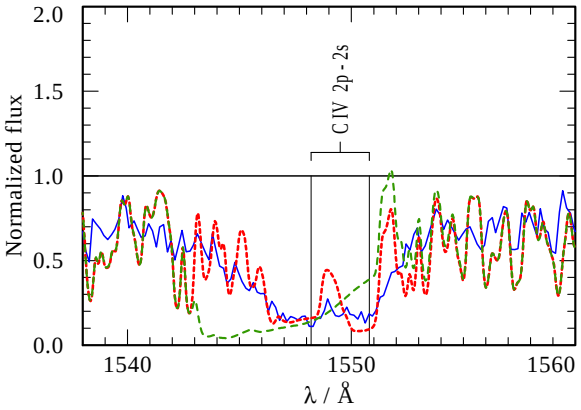

Figure 10. τ Sco: Constraining the mass-loss rate from modeling of the C IV doublet. Detail of the UV spectrum observed with IUE (blue thin line) vs. PoWR models with $\log \dot{M} = -8.6$ (green dotted line) and $\log \dot{M} = -9.3$ (red dotted line). Both models use $v_\infty = 1000$ km/s and include superionization. The C IV doublet is better matched by the model with the lower $\dot{M}$.

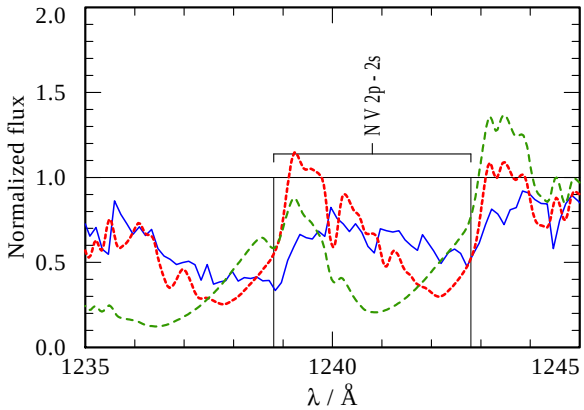

Figure 11. τ Sco: Same as in Fig. 10 but for the N V doublet. The P Cygni line profile of the N V doublet is strongly affected by X-ray ionization. The observed line is better fitted by a model with a low mass-loss rate $\log \dot{M} = -9.3$ (red dotted line).

adopted. We obtained wind parameters by modeling the C IV, N V, and Si IV lines. During our analysis we found that the line profiles in the IUE range are strongly influenced by a combination of three parameters at the same time: the terminal wind velocity v_∞, the mass-loss rate $\dot{M}$, and the impact of superionization via X-ray emission. It is not possible to disentangle these effects and therefore our solution may not be unique.

We include the X-ray flux and temperature as deduced from the observations. The need to account for X-rays in wind modeling can be nicely demonstrated using C IV and N V doublets (Figs. 6 and 7). Although it is possible to reproduce the observed C IV doublet without X-ray superionization by assuming lower $\dot{M}$ and lower v_∞, this method fails for the N V doublet. As the effective temperature of B stars is not high enough to create sufficient amounts of N V by photoionization, the observed P Cygni line profile of the N V doublet can only be reproduced if superionization due to X-rays is included. On the other hand, the Si IV doublet in τ Sco has little sensitivity to the X-rays (Fig. 8).

With fixed parameters for the X-ray emitting gas from this study, the terminal velocity of the wind can be deduced from fitting the line profiles. Fig. 9 shows the asymmetric line profile of the C IV-line doublet at $\lambda\lambda$ 1548.2, 1550.8 Å. We calculated three models taking $v_\infty = 500$, km s^{-1}, 1000 km s^{-1} and 1500km s^{-1} and keeping other parameters the same. Although a higher wind velocity cannot be excluded, we find that a model with $v_\infty = 1000$ km s^{-1} described the observed lines best.

Setting $v_\infty = 1000$ km s^{-1}, attention was next directed toward a determination of the mass-loss rate. Models with mass-loss rates in the range $\log(\dot{M}/M_\odot \mathrm{yr}^{-1})$ = -9.3 ... -8.6 were computed and compared to the UV data. We were not able to find a unique solution which could describe all lines equally well. The C IV doublet is better reproduced with lower $\dot{M} = 10^{-9.3}\, M_\odot\, \mathrm{yr}^{-1}$ as illustrated in Fig. 10. This mass-loss rate is also favored by the model fitting of the N V doublet (see Fig. 11). On the other hand, Si IV doublet is best described by a model with a higher mass loss of $\dot{M} = 10^{-8.6}\, M_\odot\, \mathrm{yr}^{-1}$ as shown in Fig. 12.

The steps as described above were performed for all our program stars.

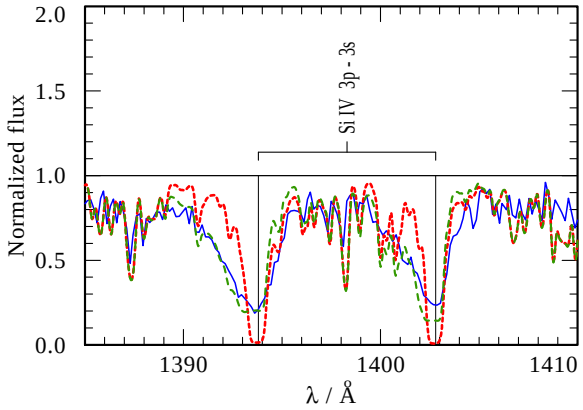

Figure 12. τ Sco: Same as in Fig. 10 and Fig. 11 but for the Si IV doublet. In contrast to the C IV and N V doublets, the observed doublet of Si IV is better matched by a model with a higher mass loss of $\log \dot{M} = -8.6$.

6.3 β Cep

β Cep is a well-studied object. Despite this, to our knowledge, there has been no prior detailed modeling of the UV resonance lines from this star. Donati et al. (2001) adopted a terminal wind velocity of $v_\infty = 900$ km s^{-1}. Using a constraint on the product $\dot{M}q$(C IV) obtained by Prinja (1989), and adopting an ionization fraction of C IV at 0.1%, Donati et al. estimated a mass-loss rate of $\log \dot{M} = -9$ for β Cep. They also noticed that this mass-loss rate is significantly lower than the predicted value of $2.4 \times 10^{-8}\, M_\odot$ yr^{-1} for a CAK model of a star like β Cep (Abbott 1982).

The ionization fractions of carbon obtained by detailed modeling of the β Cep atmosphere with the PoWR code are shown in Fig. 13. The effect of ionization by X-rays prevents C IV from being the dominant ion anywhere in the stellar wind except right at the photospheric level. Therefore systematically lower mass-loss rates would be obtained from modeling of the C IV doublet by models that do not account for the X-rays. (The effect is illustrated in Fig. 6 using τ Sco as an example.)

Schnerr et al. (2008) studied wind-line variability in magnetic B-stars. They considered all 81 UV spectra of β Cep available in the IUE archive and showed that the C IV doublet is strongly modulated with the rotation period of 12 d. Their Fig. 2 shows the gradual

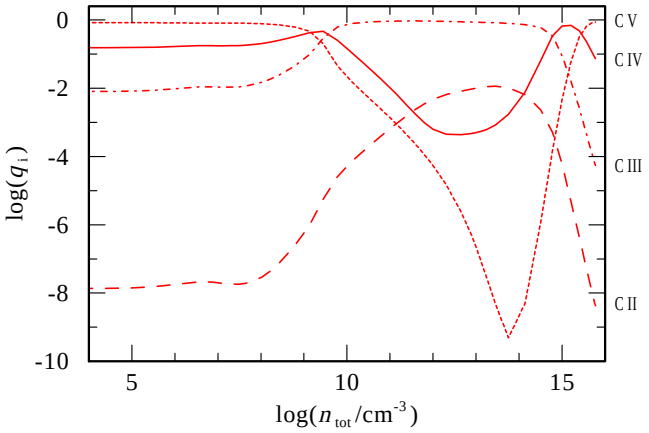

Figure 13. Relative ionization fractions of carbon in the wind of β Cep as function of density in the wind, with declining density corresponding to larger radius. The wind model is calculated with $v_\infty = 700\,\mathrm{km\,s^{-1}}$, $\log \dot{M} = -9.4$; stellar parameters are from Table 6.

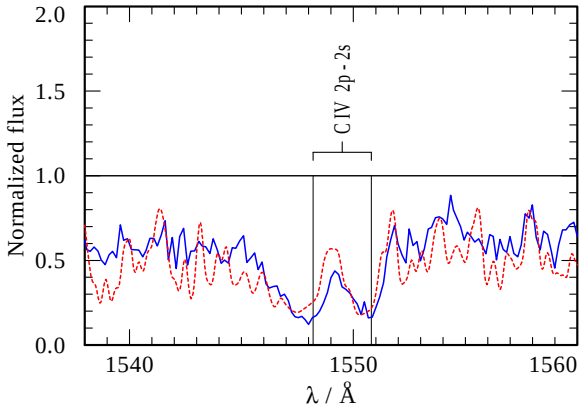

Figure 14. β Cep: Detail of the UV spectrum observed with IUE (blue thin line) vs. PoWR models with $v_\infty = 700\,\mathrm{km\,s^{-1}}$ and $\log \dot{M} = -9.4$ (red dotted line). The C IV $\lambda\lambda$1548.2, 1550.8 Å doublet is shown.

transition from an enhanced to a reduced contribution of emission centered close to zero velocity in C IV, as typical in magnetic B stars.

Figure 14 shows the observed C IV doublet compared to a model that assumes $v_\infty = 700\,\mathrm{km\,s^{-1}}$ and $\log \dot{M} = -9.4$. A higher mass-loss rate of $\log \dot{M} = -9.1$ is required to reproduce Si IV line, as shown in Fig. 15.

6.4 ξ^1 CMa

This is the first analysis of the UV spectral lines of the β Cep-type star ξ^1 CMa by means of stellar atmosphere models.

In modeling the spectrum of this object, we note that the IUE data of this star are of rather low quality. It seems that the background subtraction was not performed correctly, because the minimum of the interstellar Lyman alpha absorption line is not "black" as it should be. Therefore we adjusted the background level accordingly. Our model reproduces the broad SED from the UV to the IR very well (see Fig. 5). Figure 4 shows our model compared to the optical spectrum of ξ^1 CMa – the model produces quite a good match to the line spectra. Therefore, it is surprising that we

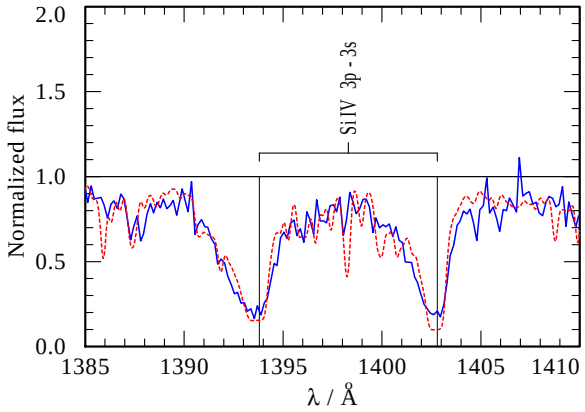

Figure 15. β Cep: The same as in Figs. 14 and but for the Si IV $\lambda\lambda$1393.8, 1402.8 Å doublet. A PoWR model with $\log \dot{M} = -9.1$ (red dotted line) is shown.

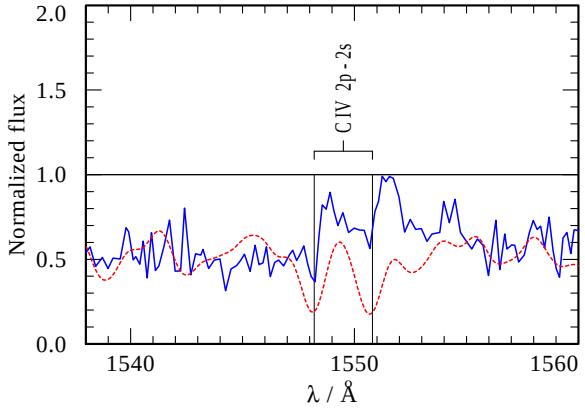

Figure 16. ξ^1 CMa: Detail of the UV spectrum observed with IUE (blue thin line) vs. PoWR models with $v_\infty = 700\,\mathrm{km\,s^{-1}}$ and $\log \dot{M} = -10$ (red dotted line). The C IV $\lambda\lambda$1393.8, 1402.8 Å doublet is shown.

were not able to achieve good quality fits to the C IV (see Figs. 16) and N V lines.

It is tempting to suggest that the reason for these modeling difficulties may be due to the pole-on orientation of ξ^1 CMa (Hubrig et al. 2011), although the poor quality of the data is a concern as well. The observed line profiles of Si IV (see Fig. 17) are roughly reproduced by our model. We adopted a larger turbulence in the wind compared to the photosphere and convolved the UV model spectra with a Gaussian of 1 Å FWHM, corresponding to a turbulence velocity of about $200\,\mathrm{km\,s^{-1}}$.

For β Cep and V2052 Oph, the mass-loss rate required to reproduce the Si IV doublet is higher as compared to what is needed to fit C IV, an effect that we attribute to the superionization by X-rays. This, however, is not the case for ξ^1 CMa. Figure 16 shows the C IV line compared to model line with $\log \dot{M} = -10$, as found from the analysis of Si IV.

Schnerr et al. (2008) presented a time-series analysis of IUE observations of the C IV doublet in ξ^1 CMa and noticed the lack of temporal modulations in the spectra. Increasing the mass-loss rate would result in a stronger absorption feature, which is not observed. Therefore, we conclude that the UV lines in ξ^1 CMa are peculiar compared to other magnetic stars in our sample, either due to the quality of the observations or reflecting intrinsic peculiarity to the source itself.

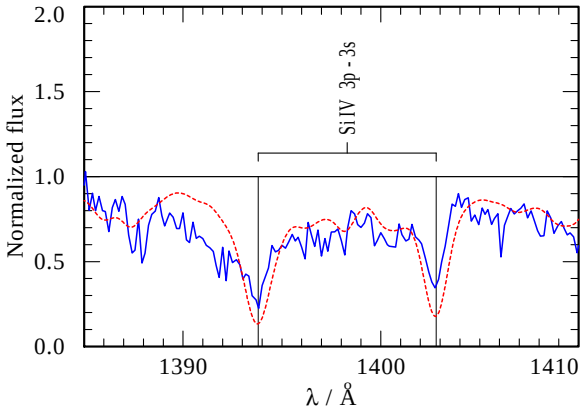

Figure 17. ξ^1 CMa: The same as in Figs. 16 but for the Si IV $\lambda\lambda$1393.8, 1402.8 Å doublet.

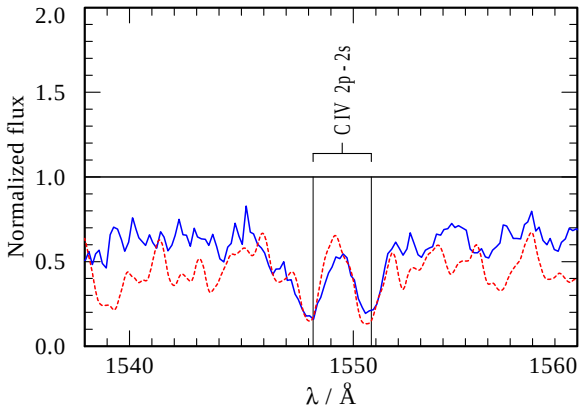

Figure 18. V2052 Oph: Detail of the UV spectrum observed with IUE (blue thin line) vs. PoWR models with $v_\infty = 700\,\mathrm{km\,s^{-1}}$ and $\log \dot{M} = -10.7$ (red dotted line). The C IV $\lambda\lambda$1548.2, 1550.8 Å doublet is shown.

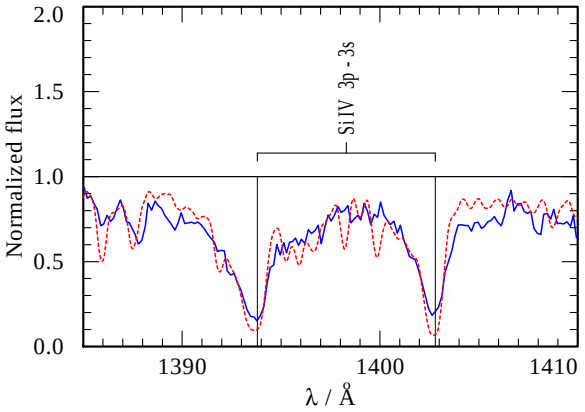

Figure 19. V2052 Oph: The same as in Fig. 18 but for the Si IV $\lambda\lambda$1393.8, 1402.8 Å doublet. A PoWR model with $v_\infty = 700\,\mathrm{km\,s^{-1}}$ and $\log \dot{M} = -9.7$ (red dotted line) is shown.

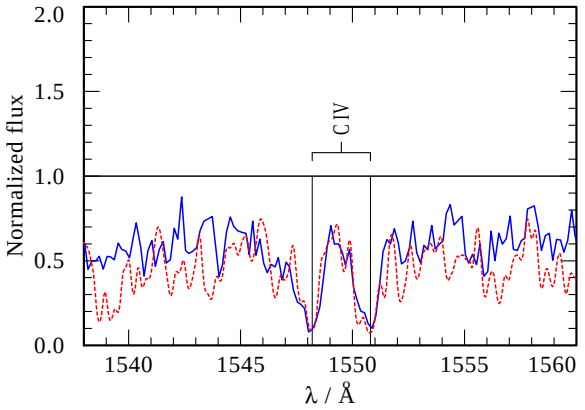

Figure 20. ζ Cas: Detail of the UV spectrum observed with IUE (blue thin line) vs. PoWR models with $v_\infty = 700\,\mathrm{km\,s^{-1}}$ and $\log \dot{M} = -11$ (red dotted line). The C IV $\lambda\lambda$1548.2, 1550.8 Å doublet shows a purely photospheric absorption profile without any wind signature.

6.5 V2052 Oph

This is the first analysis of wind properties of V2052 Oph. As with the previous stars (except τ Sco), we adopt a wind terminal velocity of $v_\infty = 700\,\mathrm{km\,s^{-1}}$. We did calculate models with $v_\infty = 1000\,\mathrm{km\,s^{-1}}$, but results were similar. Fig. 18 shows the C IV doublet in the IUE spectrum of V2052 Oph compared to a wind model with $\log \dot{M} = -10.4$. The effective temperature of V2052 Oph is relatively low at $T_{\rm eff} = 23$ kK, and C III would have been the leading ionization stage if there were no X-ray emission. As with other stars in our sample, the effect of superionization proves critical, in this case elevating the ionization fraction of C IV in the wind.

We were not able to achieve a satisfactory fit to the N V doublet with a model that includes X-ray emission. This line is very sensitive to the presence of ionizing photons in the wind, and even models with a mass loss as low as $\log \dot{M} = -10.7$ produces a N V doublet that is stronger than observed. This is an interesting challenge because the observed level of X-ray emission in V2052 Oph is quite low, smaller than in the other stars of our sample.

Similarly to results for other program stars, the Si IV doublet is better reproduced with models that assume higher mass-loss rates then required for the C IV and N V doublets. Figure 19 shows a model fit with $\log \dot{M} = -9.7$ to the Si IV lines. Note that the low $T_{\rm eff}$ of about 23 kK would normally suggest that the dominant ion stage of silicon would be Si IV; however, with the presence of X-rays, Si V becomes the dominant ion, and the Si IV doublet shows a more photospheric absorption profile.

6.6 ζ Cas

Ours is the first analysis of the wind properties of ζ Cas. This star is the coolest among our sample. Again, we fixed the parameters of X-ray emission based on *XMM-Newton* data, and calculated a range of models for various values of v_∞ and $\dot{M}$.

Figure 20 shows the observed C IV doublet plotted together with a PoWR model. The observed line shows a purely photospheric absorption profile without any wind signature and is quite well fitted with a PoWR model. From such a photospheric absorption profile, it is not possible to infer the wind velocity. We have therefore assumed a terminal wind speed of $v_\infty = 700\,\mathrm{km\,s^{-1}}$.

Wind emission signatures are present in the N V doublet as seen in Fig. 21. Note that the model N V line has a P Cygni line profile because N V becomes the leading ionization stage via the effect of superionization. However, in order to reproduce this line we have to adopt a small mass-loss rate of only $\log \dot{M} = -11$. Surprisingly, even with this mass-loss rate, the model line is somewhat stronger than observed.

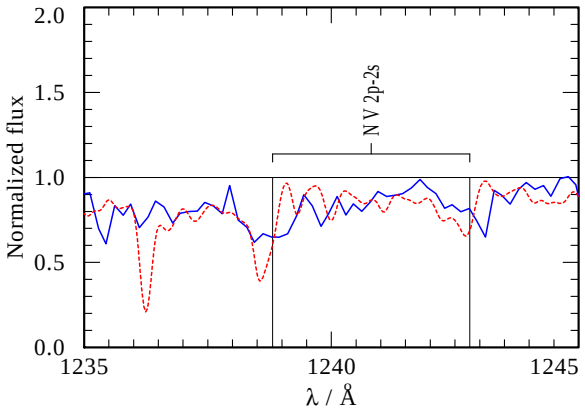

Figure 21. ζ Cas: Same as in Fig. 20 but for the N V $\lambda\lambda$1238.81, 1242.8 Å doublet.

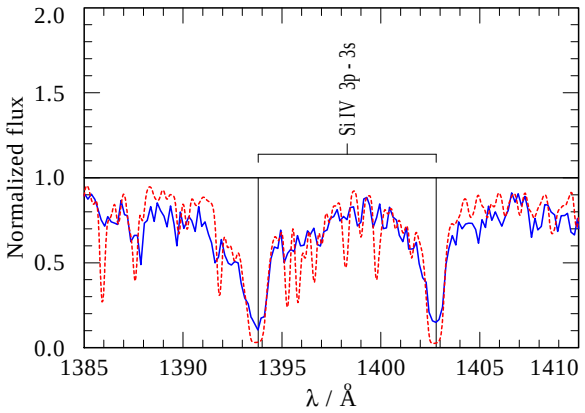

Figure 22. ζ Cas: The same as in Figs. 20 and 21 but for the Si IV $\lambda\lambda$1393.8, 1402.8 Å doublet. A PoWR model with $v_\infty = 700\,\mathrm{km\,s^{-1}}$ and $\log \dot{M} = -9.7$ (red dotted line) is shown.

Similarly to other stars, there is no unique solution for the mass-loss rate, with different UV lines indicating somewhat different mass-loss rates. Figure 22 shows models of Si IV compared with the IUE data. At a low T_* of about 21 kK, Si IV would be the dominant ion stage, but X-ray emissions make Si V the dominant ion in the wind so that the Si IV line shows a more photospheric absorption profile.

6.7 Uncertainties on $\dot{M}$ determination in non-supergiant B stars

The results of the analysis of UV and optical spectra of magnetic B stars are summarized in the Table 6. There is a discrepancy between modeling the C IV and N V doublets versus the Si IV doublet, therefore we determine the mass-loss rates in our program stars only to within a factor of a few.

The C IV, N V, and Si IV doublets differ in their sensitivity to stellar atmosphere parameters. Our models show that C IV can be the leading ionization stage in the hottest stars in our sample, such as τ Sco and ξ^1 CMa. Then X-rays destroy C IV by photoionization (see Fig. 6). (In the context of dwarf O-stars this was discussed by Martins et al. 2005; Marcolino et al. 2009). In cooler stars with $T_{\rm eff} < 27$ kK, the leading ionization stage of carbon in the wind becomes C III. In this case Auger ionization by X-rays leads to the creation of C V, followed by recombination to C IV. Therefore, the C IV line is quite sensitive to both the stellar radiation field as determined by $T_{\rm eff}$ and to the X-ray emission.

N V is not produced in the winds of stars with $T_* < 50$ kK (see Fig. 3 in Hamann & Gräfener 2004). All stars in our sample are significantly cooler, therefore the N V line in their winds originates exclusively from the ionization by X-rays. For stellar temperatures below 27 kK, the leading ion in the wind is N III, which is Auger ionized by X-rays to N V. At 27 kK and above, the leading ion is N IV. When X-rays are present in the wind, the leading ion becomes N V, or for τ Sco ($T_* = 31$ kK) even N VI.

All models that include X-ray emission and have appreciable mass-loss rates show N V with a strong P Cygni line profile, which is not observed (see Figs. 11 and 21).To achieve agreement with the observations low mass-loss rates must be adopted. For the β Cep-type variables among out program stars, the models reproduce the observed N V doublet best if the X-ray emission is "switched off". Since X-ray emission is observed, one potential explanation for curiosity could be in assuming some form of shielding of the cool stellar wind from the X-ray radiation.

The ionization of Si is also sensitive to stellar and X-ray radiative field. Models predict that in the stars with $T_* < 27$ kK, the leading ion would be Si IV, but the presence of X-rays make Si V the dominant ion. Interestingly in hotter stars with photospheric temperatures above 27 kK, the dominant ion is Si V with or without X-rays; the X-rays are not sufficient to produce a significant amount of Si VI. Let's consider β Cep and τ Sco as examples. Ignoring X-ray emission in the models, Si IV is the dominant ion in the outer wind zone, and therefore the Si IV doublet becomes asymmetric in shape. With X-rays most of the Si IV in the outer wind is destroyed (ionized to Si V), and the remaining Si IV absorption is only photospheric. On the other hand in τ Sco that is hotter, the dominant ionization stage is Si V and the Si IV line is not sensitive to the X-ray emission.

These considerations show that the stellar radiation field and the X-ray emission have to be well known to use the UV lines as mass-loss rate diagnostics. There are several factors that can influence mass-loss rate determinations, and it is worth noting these and their relative importance as briefly discussed below.

Although the stellar radiation field is well described by our models (see Fig. 4), the detailed photospheric models (e.g. Morel & Butler 2008; Morel et al. 2008)) give temperatures with uncertainties of several thousand Kelvin. Our models show that such differences in temperature are sufficient to alter the ionization stratification significantly. Thus, uncertainties in $T_{\rm eff}$ are a source of uncertainty in $\dot{M}$.

For our models we adopted abundances as derived by Morel et al. (2008). The uncertainty in abundances would reflect on the mass-loss rate determinations. However, we determine mass-loss rates only within a factor of few, which is a higher uncertainty than could be explained by the abundances.

Another source of uncertainty is represented by the spectral and spatial specifics of the X-ray radiation. From observations we constrain the X-ray flux quite well; however, the X-ray spectral distribution is only roughly known for our sources, especially for the X-ray fainter stars (see Table 3). In addition, the location of the X-ray plasma throughout the wind is unclear.

Similar to other non-LTE stellar atmosphere models, the PoWR model assumes that the statistical equilibrium is established locally. In a situation when the densities and the wind flow times are small, the timescale for recombinations can become longer than the timescale for transport by advection. In their studies of low density winds, Martins et al. (2005) tested the effects of advection and

Table 6. Stellar and wind parameters of τ Sco, β Cep, V2052 Oph, ξ^1 CMa, and ζ Cas. The highest and the lowest mass-loss rates $\dot{M}$ as obtained from the modeling of C IV and Si IV doublets for each star are given. The $\dot{M}$ value for ξ^1 CMa is as obtained from the model of the Si IV doublet only (see Section 5.4 for details). The work ratio Q (see Eq. 2 for definition) is computed for the highest mass-loss rate that is given in this table.

Star	$E_{\rm B-V}$	$T_{\rm eff}$	$\log L$	$\log g$	R	$\log \dot{M}$		v_∞	$v_{\rm esc}$	Work Ratio Q	$\log\left(\frac{L_{\rm X}}{L_{\rm bol}}\right)$
		kK	$L_\odot$	cm s^{-2}	$R_\odot$	$[M_\odot\,{\rm yr}^{-1}]$		km s^{-1}	km s^{-1}		
						C IV	Si IV				
τ Sco	0.03	30.7	4.3	3.97	5.0	-9.3	-8.6	1000	810	2	-6.4
β Cep	0.03	25.1	4.2	3.62	7.0	-9.4	-9.1	700	640	3	-7.0
ξ^1 CMa	0.04	27.0	4.5	3.7	8.2		-10	700	750	14	-6.6
V2052 Oph	0.26	23.0	3.9	4.0	5.7	-10.7	-9.7	700	900	3	-8.0
ζ Cas	0.04	20.9	3.7	3.7	5.4	-11.0	-9.7	700	620	2	-7.5

adiabatic cooling on the ionization structure and the UV lines for a star with $\log \dot{M} \approx -9$. They found that the inclusion of these effects would result in an increase of the empirically derived log $\dot{M}$ by $\sim$0.15. This is within the error margin of the $\dot{M}$ derived for our sample stars. It is also important to notice that our final results are based on unclumped wind models. If the winds are clumped, the recombination time scale in dense clumps becomes shorter. As a test we calculated a grid of models that account for microlumping for β Cep. However, no significant difference was found compared to the un-clumped models. Moreover, in our models, the N V and C V produced via Auger ionization are the leading ionization stages, therefore our assumption of local ionization balance does not introduce a large error in the model ionization structure.

We assume a spherically symmetric winds. Except τ Sco that has a complex magnetic topology, the stars in our sample are oblique magnetic rotators. Their winds are likely confined by magnetic fields, therefore, the treatment by the spherically symmetric models can be a source of uncertainty.

Four of our program stars are β Cep type stars. As noticed by Donati et al. (2001), in principle, the mass-loss rate may change by $\approx$ 20% in response to the $\approx$ 9% pulsation-induced luminosity changes, while the terminal velocity should remain roughly constant. However, these changes in the $\dot{M}$ are within the errors of our estimates.

Ultimately it appears that better determinations of the effective photospheric temperature along with a better understanding of the flow structure and X-ray sources in the systems will be needed to obtain consistent mass-loss rates that result in self-consistent fits for all of the UV wind lines.

6.8 The weak wind problem

It is known that O-type dwarfs with luminosities $\log L/L_\odot \lesssim 5.2$ have mass-loss rates that are orders of magnitude lower than predicted by the CAK theory (see Marcolino et al. (2009) and references therein). This discrepancy is commonly refereed to as "the weak-wind problem".

Babel (1996) refined the CAK theory for the B-type stars by studying the theoretical effects of shadowing by photospheric lines on radiative acceleration. It was shown that these effects have large consequences on the winds of main sequence B stars. In particular, the main difference from the predictions of the CAK theory is found for stars with $T_{\rm eff} \approx 20000 - 23000$ K and $\log g \approx 3.7 - 4.0$. For these objects, the mass-loss rate is found to be lower than predicted by CAK theory by at least a factor of 4. Among the stars in our sample, ζ Cas has values of $T_{\rm eff}$ and $\log g$ for which the theoretical wind models were computed by Babel (1996). The predicted mass-loss rate for this star is $10^{-8.8}\,M_\odot\,{\rm yr}^{-1}$with a terminal wind velocity of $v_\infty = 3.4 v_{\rm esc}$ (compared to $\log \dot{M} = -8.2$, $v_\infty = 1.8 v_{\rm esc}$ as predicted by the CAK theory).

Our results show that the mass-loss rate in ζ Cas does not exceed $10^{-9.7}\,M_\odot\,{\rm yr}^{-1}$. This is ≈ 8 times smaller that the prediction of Babel (1996). Furthermore, we do not find any evidence for the predicted fast wind velocity of $v_\infty = 2100$ km s^{-1}. Similarly, for all other stars in our sample, the mass-loss rates are an order of magnitude lower than predictions by Abbott (1982) based on the CAK theory. The discrepancy with the predictions of Vink et al. (2000) is even larger. Thus we conclude that all stars in our sample belong to the category of weak-wind stars. [2]

This conclusion is corroborated by the high *work ratio* Q we find in our program stars (see Table 6). As the work ratio Q we define the mechanical work per unit time done by the radiation field compared to the mechanical luminosity of the wind., The exact definition of Q as computed in the PoWR code is

$$Q \equiv \frac{\int_r \left[g_{\rm rad}(r) - \frac{1}{\rho(r)} \frac{{\rm d}P_{\rm g}}{{\rm d}r} \right] {\rm d}r}{\int_r \left[v \frac{{\rm d}v}{{\rm d}r} + \frac{GM_*}{r^2} \right] {\rm d}r}, \qquad (2)$$

where $g_{\rm rad}$ is the radiative acceleration, $P_{\rm g}$ is the gas pressure, and other symbols have their usual meanings. In a hydrodynamically consistent model $Q = 1$. When $Q > 1$ the model predicts that there is sufficient line opacity to produce radiative acceleration that is capable to drive stronger wind than the observed from the UV resonant doublets. We calculated hydrodynamically consistent models by choosing $\dot{M}$ values that that yield work ratios of $Q \approx 1$. Such models yield $\log \dot{M}(Q \approx 1) = -9.4$ for V2052 Oph and $\log \dot{M}(Q \approx 1) = -8.2$ for ξ^1 CMa.

Importantly, these work ratios Q are calculated from models that include X-ray emission in the ionization balance. Drew et al. (1994) highlighted the effect that X-ray emission may have on the wind velocity and mass-loss rate. They suggest that ionization by X-rays may change the ionization structure in the inner part of the wind, thus reducing the total radiative acceleration and consequently the mass-loss rate. Our models include the ionization by X-rays in the wind acceleration zone at the level and temperatures indicated by the X-ray observations. Yet, we find that there is still sufficient radiative acceleration to drive mass-loss in excess of the value inferred from the UV line-fitting analysis. Therefore, the ionization by X-rays cannot be the unique solution of the weak-wind problem.

Cassinelli et al. (1994), Cassinelli (1994), Cohen et al. (1997)

[2] Recently Lucy (2010) identified a weak-wind domain on a $\log g$–$\log T_{\rm eff}$ diagram where a star's rate of mass loss by a radiatively-driven wind is less than that due to nuclear burning. All our program stars belong to this domain.

studied the X-ray emission from near-main sequence B-type stars based on *Rosat* data. They found that these stars show departure from the $L_{\rm X} \approx 10^{-7} L_{\rm bol}$ law which holds for O-type stars. From evaluating the emission measure of X-ray emitting gas, they concluded that a major fraction of the wind emission measure is hot, whereas in shocked wind theory less than 10 percent of the wind emission measure should be hot.

Our observations and models support these conclusions. The models show that the Emission Measure 'filling factor' of the hot material (as determined from X-ray observations) relative to the cool wind $X_{\rm fill}$ exceed unity for all our stars. While $X_{\rm fill} \approx 8$ for τ Sco is smallest, it is as large as $X_{\rm fill} \approx 200$ for ζ Cas and extremely large $X_{\rm fill} \approx 1000$ for ξ^1 CMa. Thus, not only are the UV lines in ξ^1 CMa the most difficult to reproduce from the models, its X-ray filling factor and wind work ratio Q are also outstandingly high.

The high X-ray filling factors imply that either the hot gas $EM_{\rm hot}$ occupies a much larger volume than the cool wind $EM_{\rm cool}$ where the UV lines are formed, or that the X-ray emitting gas has higher density. Both possibilities seem plausible in the case of magnetic stars. The cool wind can occupy a relatively smaller volume because it emerges primarily from the magnetic polar regions in stars with dipole fields. On the other hand, high density hot plasma can occur in magnetically confined wind zones or loops.

7 DISCUSSION

7.1 X-ray emission from magnetic early-type B stars

One of the results of our study is that X-ray properties of newly discovered magnetic B-type stars are diverse. Except for τ Sco and ξ^1 CMa, our program stars are not especially X-ray luminous. On the contrary, V2052 Oph and ζ Cas are intrinsically X-ray faint. Can these differences in luminosity be explained in the framework of the MCWS model? Babel & Montmerle (1997b) obtained a simple scaling relation between X-ray luminosity and the magnetic and stellar wind parameters in the framework of their MCWS model. They predicted that the X-ray luminosity scales approximately with the product of wind momentum and some power of the magnetic field strength, $L_{\rm X} \propto B^{0.4} \dot{M} v_\infty$ (see their Eqs. (10)–(11)). We apply this scaling relation to predict X-ray luminosities for our sample stars with dipole magnetic fields. Among our sample stars, ξ^1 CMa has the strongest magnetic field, while its wind momentum is comparable to other stars. The scaling relation of Babel & Montmerle (1997b) predicts rather weak dependence on the magnetic field strength. The predicted value of $L_{\rm X}$ (4×10^{30} erg s^{-1}) is an order of magnitude lower that the observed. On the other hand, V2052 Oph and ζ Cas have a low wind kinetic energy and a weak magnetic field. Using the lower values of $\dot{M}$ from Table 6, the predicted X-ray luminosities for these stars ($\approx$ few $\times\, 10^{29}$ erg s^{-1}) agrees well with the observed ones. Similarly, for the lower value of $\dot{M}$ for β Cep, the predicted and observed luminosities agree quite well. Thus, the basic scalings obtained by Babel & Montmerle (1997b) for the X-ray luminosity can qualitatively explain the difference in the level of X-ray luminosity among β Cep, V2052 Oph, and ζ Cas. Note, however, that using the upper values for $\dot{M}$ for these stars in the Babel & Montmerle (1997b) scaling relation, would result in the X-ray luminosities that are too high compared to the observed ones.

The more serious challenge is to understand the comparatively low temperatures of X-ray emitting plasma obtained from the analyses of the observed spectra and the lack of time modulations of the X-ray flux. The X-ray spectral temperatures of magnetic B-stars in our sample are not especially high. ζ Cas has one of the softest X-ray spectra among those measured in OB stars. Moreover, X-ray emissions from both τ Sco and β Cep were monitored throughout a rotation period, and neither display rotational modulations in their X-ray light curves (Favata et al. 2009; Ignace et al. 2010).

Compared to non-magnetic stars, the harder X-ray spectrum and rotationally modulated X-ray variability are predicted by *different* models of hot plasma production in magnetically confined winds (e.g. Li et al. 2008; Gagné et al. 2005). Can these models, which assume that wind motion is governed by the magnetic field, be applied to our program stars?

It is usual to describe the relative importance of magnetic fields in gases by the plasma-β parameter with $\beta_{\rm p} = 8\pi p/B^2$, where p is the gas pressure. The gas is magnetically dominated when $\beta_{\rm p} < 1$.

For supersonic flows such as stellar winds the ram pressure exceeds the gas pressure and the dynamical importance of a magnetic field is defined by the ratio of wind kinetic to magnetic energy density, given by the supersonic flow β viz. $4\pi\rho v^2/B^2$, where v is the supersonic flow speed. A small or large value indicates whether the magnetic field locally dominates the bulk motion, or vice versa. Supersonic rotation can be treated similarly (e.g. Brown et al 2008). Specifically Altschuler & Newkirk (1969, and ref. therein) show that beyond the *Alfvén* radius $R_{\rm A}$, where

$$B^2/8\pi = \rho v^2/2 \tag{3}$$

is met, the radial stellar wind forces magnetic field lines to to become approximately radial. By contrast for $R < R_{\rm A}$, the wind flow is confined by the magnetic field.

In the context of stellar winds, wind confinement was considered by Babel & Montmerle (1997), ud-Doula & Owocki (2002), Brown et al (2008) and others. Recalling that the wind density $\rho = \dot{M}/4\pi v(R) R^2$, one can express $R_{\rm A}$ from the condition set by Eq. (3):

$$R_{\rm A} = \sqrt{\frac{\dot{M} v(R)}{B^2}}. \tag{4}$$

In case of a dipole magnetic field $B = B_0 (R_*/R)^3$ Eq. (4) can be re-written as

$$r_{\rm A} \cdot w(r)^{\frac{1}{4}} = \left(\frac{R_*^2 B^2}{\dot{M} v_\infty} \right)^{\frac{1}{4}} \equiv \eta_*^{\frac{1}{4}}, \tag{5}$$

where $r = R/R_*$, and the standard parametric wind velocity law with $v(r) = v_\infty (1 - r^{-1})^\beta \equiv v_\infty w(r)$ is assumed. It is convenient to express η_* in terms of normalized stellar wind parameters, with $\dot{M}_{-9}$ the mass loss rate in units of $10^{-9} M_\odot$ yr^{-1}, v_∞ in km s^{-1}, and $\mathcal{R}_*$ the radius in units of solar radius $R_\odot$. Then

$$\eta_* \approx 1 \cdot \frac{\mathcal{R}_*^2}{\dot{M}_{-9} v_\infty} \cdot B_0^2. \tag{6}$$

For stars with dipole fields (i.e. excluding τ Sco) the field strength at the magnetic pole is shown in Table 6. To estimate $r_{\rm A}$ we use as a characteristic value the field strength at the magnetic equator (i.e. half of the polar field strength). Then we find $\eta_*(\beta\,\text{Cep}) \gtrsim 3\times10^3$, $\eta_*(\xi^1\,\text{CMa}) \approx 6\times10^6$, $\eta_*(\text{V2052 Oph}) \gtrsim 4\times10^3$, and $\eta_*(\zeta\,\text{Cas}) \gtrsim 6\times10^3$. Consequently, the Alfvén radius is at $\approx 50\,R_*$ for ξ^1 CMa and $\lesssim 10\,R_*$ for other stars. These estimates are based on the highest mass-loss rates obtained from fitting of the UV lines.

However, we know that a significant fraction of the wind mass loss can be in the form of hot X-ray emitting plasma. We may hypothesize that the "true" total amount of matter is much higher. We calculated a hydrodynamically consistent model for V2052 Oph and ξ^1 CMa (see Section 6.8) to obtain a mass-loss rate $\log \dot{M}(Q \approx 1) = -9.4$ for the former and $\log \dot{M}(Q \approx 1) = -8.2$ for the latter. Even with these higher mass-loss rates, the magnetic fields regulate the wind motion up to $\approx 7\,R_*$ for V2052 Oph and $\approx 20\,R_*$ for ξ^1 CMa.

Thus the winds of our sample stars are strongly confined out to several stellar radii where the wind velocity should reach its terminal value. Due to the very weak signatures of the winds seen in the UV line profiles, we can establish v_∞ only with a limited degree of accuracy. Using $v_\infty \approx 700\,\mathrm{km\,s^{-1}}$ is reasonably consistent with the UV lines. Colliding wind streams at such a speed from two opposite directions of the magnetosphere should produce strong shocks, heating plasma up to ≈ 20 MK. This is far above the maximum temperatures we infer from the spectral analysis (see Table 3).

From the UV line modeling, we cannot exclude somewhat lower v_∞ for the winds of our stars, which would alleviate the expectation of very hot temperatures, scaling as v_∞^2. However, there is, perhaps, a more severe problem of the differential emission measure distribution (DEM). The emission measure of the hottest plasma is $\approx$ 35% of the total EM in ξ^1 CMa and only ≈10% in β Cep. On the other hand, the plasma with the largest emission measure has a temperature of only about 1.3 MK in ξ^1 CMa (see Table 3). This dominant contribution to the DEM from the cooler hot gas component is in apparent contradiction with the predictions of the MCWS models, where the DEM is expected to peak at the hottest temperature (e.g. see Fig. 8 in Nazé et al. 2010).

What could be the source of wind heating in magnetic β Cep-type stars? As pointed out by Favata et al. (2009), the relatively low temperature of the X-ray emitting plasma and the absence of flares makes heating due to magnetic reconnection in analogy to active cool stars rather implausible. Heating by wind shocks owing to the intrinsic LDI mechanism in radiatively driven winds is a possibility. However, the LDI needs further theoretical study in relation to its operation in complex geometries and the dynamics of magnetically confined winds.

Another possibility could be heating by the deposition of mechanical energy related to stellar pulsations. Cassinelli et al. (1996) found from EUVE observations that the β Cep-type star β CMa has an EUV exceeding atmosphere model predictions by an order of magnitude. [3]. They suggest that this may be related to the presence of heated regions near the stellar surface owing to pulsations and magnetic fields. If the upper atmosphere is heated mechanically by pulsational effects, it is likely that the X-ray source regions are also heated by a related mechanism. In this case, the dynamic time scale of the wind is smaller than the time required to establish ionization equilibrium.

To investigate this possibility, we show in Fig. 23 the X-ray luminosities versus pulsation periods and amplitudes for few prominent β Cep-type variables. Given the small sample it is difficult to draw any conclusions, yet there is no apparent dependence of the X-ray luminosity on period or pulsational amplitude.

[3] It is possible that this problem can be resolved by a better description of X-ray emission in model atmospheres (Hamann et al., in prep.).

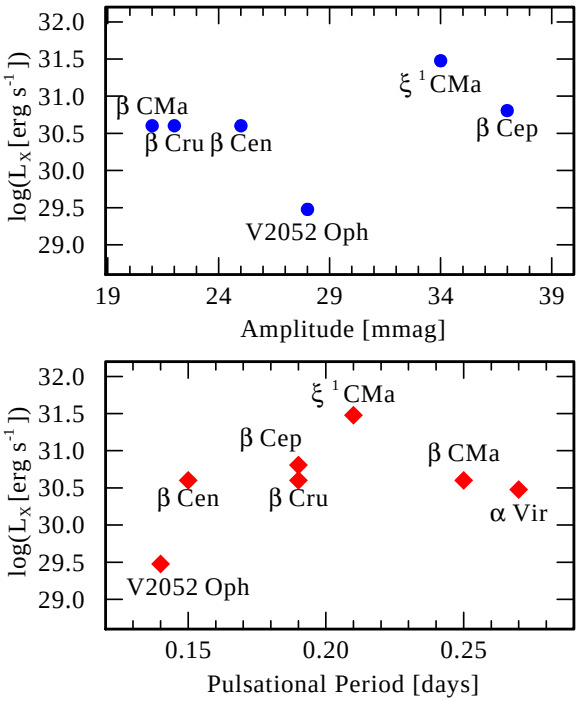

Figure 23. X-ray luminosity of some prominent β Cep-type stars vs. magnitude of pulsation (upper panel) and pulsational period (lower panel) from the catalog of Stankov & Handler (2005).

7.2 Comparison of X-ray properties between B stars with and without confirmed magnetic fields

In this section we compare X-ray properties of "normal" early-type B stars where magnetic fields have not been detected up to now. The *XMM-Newton* spectrum of the β Cep-type variable β Cen (B1III) is well fitted with a three temperature spectral model, with the hottest component $kT_{\max} \approx 0.6$ keV and $\langle kT \rangle = 0.3$ keV (Raassen et al. 2005). Hubrig et al. (2006) and Silvester et al. (2009) searched for a magnetic field in the β Cep-type β CMa (B1II-III) and did not detect magnetism, with errors on a longitudal field of just 10 G. β CMa was observed by *XMM-Newton*, its spectrum is well described by a multi-temperature model with the hottest temperature component at $kT = 0.3$ keV (Waldron et al. 2011, in prep.). *Chandra* LETGS spectrum of α Vir (B1III-IV) was analyzed in Zhekov & Palla (2007), who report the maximum of the emission measure distribution as being between 0.2 keV and 0.3 keV. We obtained LETGS *Chandra* observations of α Cru (B0.5IV). Its X-ray temperature and luminosity are similar to those of α Vir (Ignace et al. in prep.). β Cru is another B1 giant observed by *Chandra*. Zhekov & Palla (2007) find the maximum of the emission measure distribution in this β Cep-type variable is between 0.2 keV and 0.3 keV. Thus, it appears that X-ray luminosities and temperatures are very similar among the β Cep-type stars.

On the other hand, the X-ray luminosities of magnetic stars have much greater dispersion, with two significant outliers: the X-ray luminous ξ^1 CMa and the X-ray faint V2052 Oph, while their spectral X-ray temperatures are rather similar (see Table 3). Due to the small number of stars included in our investigation, this conclusion is only preliminary. Larger samples need to be considered to draw firm conclusions about the differences in X-ray properties of magnetic and "normal" early-type B stars.

Overall, it has emerged from our analysis that high X-ray lu-

minosity and hard X-ray spectra are not necessary observational characteristics of the magnetic early-type stars. This conclusion fully confirms the earlier results based on the RASS data (see also recent results on X-rays from A0p stars (Robrade & Schmitt 2011)).

One of the complications in massive early-type star studies is that a significant fraction of such stars is in binary or multiple systems and may have spatially unresolved companions that are intrinsic X-ray sources. An X-ray source spatially coincident with a B star can be due to a lower mass companion (Czesla & Schmitt 2007; Remage Evans et al. 2011). In this paper we consider B0-B2 type stars. These stars are young, not older that a few 10 Myr. Possible low-mass companions would be coronally active with X-ray luminosities of 10^{28}–10^{30} erg s^{-1} (e.g. Flaccomio et al. 2003). Two newly X-ray detected stars considered in this paper, V2052 Oph and ζ Cas, have X-ray luminosities in this range (see Table 4). Therefore, in principle, we cannot rule a confusion with an unseen coronal component. Nevertheless, we have strong indications that the observed X-ray emission is intrinsic for the early-type B stars. The spectra of X-ray emission from ζ Cas and V2052 Oph are soft, e.g. in ζ Cas the average temperature is 1 MK. This is not usual for young T Tau type stars, which have average temperatures in the range 5–30 MK (Güdel & Nazé 2009). The temperature of the X-ray emitting plasma in V2052 Oph is similar to other β Cep-type stars, albeit its X-ray luminosity is quite low (see Fig. 23). From the analysis of the UV spectra of our program stars, we know that X-rays are present in the winds since they are required to enhance the fraction of C IV and N V in the winds (see Sect. 6.5). On this basis, we believe that the observed X-ray emission is intrinsic for β Cep, V2052 Oph, ζ Cas, and ξ^1 CMa. Among stars in our sample, β Cep is a known binary star with a late Be-type companion. Late Be stars are not known to be intrinsic X-ray sources, therefore it seems reasonable to assume that the observed X-ray emission is intrinsic to the B2 component.

7.3 X-rays in stars with very small $\dot{M}$

ζ Cas displays quite a soft X-ray spectrum with nearly 85% of the EM at temperature $\lesssim$1 MK (Fig. 3 and Table 3). Our estimate of its mass-loss rate ($\dot{M} \sim 10^{-11}\,M_\odot\,\mathrm{yr}^{-1}$) places this object in the regime where the winds may display unusual properties.

Springmann & Pauldrach (1992) demonstrated that the assumption of a one-component fluid will not be valid for low density winds. Instead, the metal ions lose their dynamical coupling to the ions of hydrogen and helium. The metal ions will move with high velocities, with helium and hydrogen failing to be dragged along. The collisionally induced momentum transfer is accompanied by frictional heating, which dominates the energy balance. As a result, Springmann & Pauldrach (1992) predict electron temperatures of $T \sim 1$ MK in the outer wind regions for stars with mass-loss rates of $\approx 10^{-8\ldots9}\,M_\odot\,\mathrm{yr}^{-1}$. The subsequent analysis of Krtička & Kubát (2000) and Owocki & Puls (2002) favored even weaker winds with $\dot{M} \sim 10^{-11}\,M_\odot\,\mathrm{yr}^{-1}$ for the wind decoupling to occur.

The theoretical analysis of this problem is not settled (e.g. Votruba et al. 2007). Gayley & Owocki (1994) investigated the effects of "Doppler heating" in stars with low mass-loss rates, and confirmed the conclusions of Springmann & Pauldrach (1992). They also noticed that Doppler heating may lead to an instability, possibly resulting in a larger degree of microturbulence. This is an interesting prediction since our analysis favors large microturbulent broadening, as in the case of ξ^1 CMa.

Given its small $\dot{M}$ value and very soft X-ray spectrum, it is tempting to suggest that ζ Cas may be a candidate object for wind decoupling.

Another interesting mechanism for generating X-ray emission in rotating magnetic stars was put forward by Suzuki et al. (2006). They proposed that extended X-ray-emitting regions can exist in massive stars with thin winds owing to collisionless damping of fast MHD waves. Stellar rotation causes magnetic field lines anchored at the stellar surface to form a spiral pattern, and magneto-rotational winds can be driven (e.g., Weber & Davis 1967). If the structure is magnetically dominated, fast MHD waves generated at the surface can propagate almost radially outward and cross the field lines. The propagating waves undergo collisionless damping owing to interactions with particles surfing on magnetic mirrors that are formed by the waves themselves. The dissipation of the wave energy produces heating and acceleration of the outflow. The Suzuki et al. (2006) mechanism works effectively in moderate and fast rotating stars. Considering Figure 6 in Suzuki et al. (2006), the magnetic field strength, wind density, and rotation speed in ζ Cas are such that the star may be in the domain where the Suzuki et al. mechanism is operational.

7.4 On the multi-phase structure of winds from magnetic early B-type stars

We try to understand whether some of the facts that have emerged from our analysis can be qualitatively explained by a picture of an oblique magnetic rotator where the bulk of the stellar wind is governed by the dipole magnetic field.

Despite relatively strong surface fields, oblique magnetic rotators have open field regions near their magnetic poles, and thus may have sectors of wind flow that are similar to normal B type stars. The UV spectra could originate in these cool sectors of the wind with a smaller filling factor as compared to the hot gas. The wind distribution is clearly asymmetric (not even axisymmetric owing to rotation). Perhaps this could explain the strange properties of the UV lines seen in ξ^1 CMa that we view nearly rotational pole-on to the rotation axis, and possibly the large dispersion in X-ray luminosities among our sample stars as well.

The hot part of the wind is apparently heated up to a few MK. This matter is confined by the magnetic field up to $10\,R_*$, so it occupies a large volume, and, in parts, may have high density. This would explain the large filling factors of hot material we infer from our models. The spatial separation between hot and cool gas may explain how the observed N V doublet can be weaker than predicted by our stellar atmosphere models. The total amount of matter in the cool and hot wind components may be close to values predicted by our hydrodynamically consistent models, and so the "true" mass-loss rates are a factor of a few higher than obtained from the empirical fits of UV lines using a model that relies on spherical symmetry.

8 SUMMARY OF RESULTS

Dedicated *XMM-Newton* observations were obtained for three early-type magnetic B-type stars, ξ^1 CMa, V2052 Oph, and ζ Cas. We report first detections of X-ray emission from V2052 Oph and ζ Cas. The observations show that the low-resolution X-ray spectra of our program stars are well described by a multi-temperature CIE plasma. The bulk of the emission measure originates from the plasma with a temperature of $\approx$ 1 MK. The X-ray luminosities dif-

fer by large factors, with ξ^1 CMa being the most X-ray luminous star in our sample, and V2052 Oph the least luminous.

We compare X-ray properties of β Cep-type variables that have magnetic field detections against those without such detections. Our comparison shows indications that the general X-ray properties are quite similar, although the magnetic stars display a greater dispersion in their X-ray luminosities. We searched for correlations between X-ray emission and pulsational and rotational properties of the stars but were not able to find any. Larger samples need to be studied to draw firm conclusions.

The basic MCWS model scaling relation between X-ray luminosity and stellar magnetic field and wind parameters (Babel & Montmerle 1997b) qualitatively describes the difference in the observed level of X-ray emission from our sample stars.

We compiled a sample of peculiar early B-type magnetic stars and considered their X-ray properties based on archival data. The comparison shows that these stars, despite very similar stellar and magnetic field parameters, have quite different X-ray properties: while some stars are hard and luminous X-ray emitters, others are apparently soft and rather faint. This new data confirm earlier results based on studies of Ap-Bp stars using RASS data.

We analyzed spectra of five non-supergiant B stars with magnetic fields by means of non-LTE comprehensive stellar atmosphere code PoWR. The PoWR models accurately fit the stellar photospheric spectra and also accurately reproduce the SED from the UV to the IR band.

The PoWR code was used to empirically obtain wind parameters of τ Sco, β Cep, ξ^1 CMa, V2052 Oph, and ζ Cas from the analysis of C IV, N V, and Si IV doublets in stellar UV spectra.

The model UV lines depend sensitively on the parameters of X-ray emission, wind velocity, and mass-loss rate. X-ray properties as derived from the observed spectra were incorporated into the wind models. We confirm that the emission measure filling factors of X-ray emitting material are high, exceeding unity for all stars.

Our analysis revealed the weak wind problem for the magnetic early type B stars. The wind terminal speeds are on the order of stellar escape speed. The inferred mass-loss rates from the UV line analyses are significantly lower than the theoretically expected and predicted by hydrodynamically consistent wind models.

Although X-rays strongly impact the ionization structure in the wind, their effect does not reduce the total radiative acceleration enough to explain the low mass-loss rates deduced from modeling the UV lines. When X-rays at the observed level and temperatures are included in the model, there is still sufficient radiative acceleration to drive a stronger mass-loss than the observed one.

ACKNOWLEDGMENTS

Based on observations obtained with *XMM-Newton*, an ESA science mission with instruments and contributions directly funded by ESA Member States and NASA. We are grateful to Nolan Walborn for his comments on the manuscript and his advice on the spectral classification of our sample stars. We are also indebted to the referee, Stephen A. Drake, for very useful comments that helped to improve the clarity of the paper, and for pointing out some aspects in the studies of magnetic stars that we did not consider in the original manuscript. This research has made use of NASA's Astrophysics Data System Service and the SIMBAD database, operated at CDS, Strasbourg, France. Funding for this research has been provided by NASA grant NNX08AW84G (RI), DLR grant 50 OR 0804 (LMO) and a UK STFC Grant (JCB).

REFERENCES

Abbott D. C., 1982, ApJ, 259, 282
Abt H. A., Levato H., Grosso M., 2002, ApJ, 573, 359
Altschuler M. D., Newkirk G., 1969, Sol. Phys., 9, 131
Arnaud K. A., 1996, in Astronomical Society of the Pacific Conference Series, Vol. 101, Astronomical Data Analysis Software and Systems V, G. H. Jacoby & J. Barnes, ed., pp. 17–+
Asplund M., Grevesse N., Sauval A. J., Scott P., 2009, ARA&A, 47, 481
Babel J., 1996, A&A, 309, 867
Babel J., Montmerle T., 1997a, ApJ, 485, L29+
—, 1997b, A&A, 323, 121
Baum E., Hamann W.-R., Koesterke L., Wessolowski U., 1992, A&A, 266, 402
Bohlender D. A., Landstreet J. D., Brown D. N., Thompson I. B., 1987, ApJ, 323, 325
Borra E. F., Landstreet J. D., 1979, ApJ, 228, 809
Brown J. C., Cassinelli J. P., Maheswaran M., 2008, ApJ, 688, 1320
Bychkov V. D., Bychkova L. V., Madej J., 2003, A&A, 407, 631
Cardelli J. A., Clayton G. C., Mathis J. S., 1989, ApJ, 345, 245
Cash W., 1979, ApJ, 228, 939
Cassinelli J. P., 1994, Ap&SS, 221, 277
Cassinelli J. P., Brown J. C., Maheswaran M., Miller N. A., Telfer D. C., 2002, ApJ, 578, 951
Cassinelli J. P., Cohen D. H., Macfarlane J. J., Drew J. E., Lynas-Gray A. E., Hubeny I., Vallerga J. V., Welsh B. Y., Hoare M. G., 1996, ApJ, 460, 949
Cassinelli J. P., Cohen D. H., Macfarlane J. J., Sanders W. T., Welsh B. Y., 1994, ApJ, 421, 705
Cassinelli J. P., Olson G. L., 1979, ApJ, 229, 304
Cohen D. H., Cassinelli J. P., Macfarlane J. J., 1997, ApJ, 487, 867
Czesla S., Schmitt J. H. H. M., 2007, A&A, 465, 493
Donati J., Babel J., Harries T. J., Howarth I. D., Petit P., Semel M., 2002, MNRAS, 333, 55
Donati J., Howarth I. D., Jardine M. M., Petit P., Catala C., Landstreet J. D., Bouret J., Alecian E., Barnes J. R., Forveille T., Paletou F., Manset N., 2006, MNRAS, 370, 629
Donati J., Landstreet J. D., 2009, ARA&A, 47, 333
Donati J., Wade G. A., Babel J., Henrichs H. f., de Jong J. A., Harries T. J., 2001, MNRAS, 326, 1265
Drake S. A., Linsky J. L., Schmitt J. H. M. M., Rosso C., 1994, ApJ, 420, 387
Drew J. E., Hoare M. G., Denby M., 1994, MNRAS, 266, 917
Dziembowski W. A., Pamiatnykh A. A., 1993, MNRAS, 262, 204
Favata F., Neiner C., Testa P., Hussain G., Sanz-Forcada J., 2009, A&A, 495, 217
Feldmeier A., Kudritzki R., Palsa R., Pauldrach A. W. A., Puls J., 1997a, A&A, 320, 899
Feldmeier A., Puls J., Pauldrach A. W. A., 1997b, A&A, 322, 878
Ferrario L., Pringle J. E., Tout C. A., Wickramasinghe D. T., 2009, MNRAS, 400, L71
Flaccomio E., Damiani F., Micela G., Sciortino S., Harnden Jr. F. R., Murray S. S., Wolk S. J., 2003, ApJ, 582, 398

Gagné M., Oksala M. E., Cohen D. H., Tonnesen S. K., ud-Doula A., Owocki S. P., Townsend R. H. D., MacFarlane J. J., 2005, ApJ, 628, 986
Gayley K. G., Owocki S. P., 1994, ApJ, 434, 684
Getman K. V., Flaccomio E., Broos P. S., Grosso N., Tsujimoto M., Townsley L., Garmire G. P., Kastner J., Li J., Harnden Jr. F. R., Wolk S., Murray S. S., Lada C. J., Muench A. A., McCaughrean M. J., Meeus G., Damiani F., Micela G., Sciortino S., Bally J., Hillenbrand L. A., Herbst W., Preibisch T., Feigelson E. D., 2005, ApJS, 160, 319
Gräfener G., Koesterke L., Hamann W., 2002, A&A, 387, 244
Groote D., Hunger K., 1982, A&A, 116, 64
Groote D., Schmitt J. H. M. M., 2004, A&A, 418, 235
Grunhut J. H., Wade G. A., Rivinius T., Marcolino W. L. F., Townsend R., the MiMeS Collaboration, 2010, ArXiv e-prints
Güdel M., Nazé Y., 2009, A&A Rev., 17, 309
Hamann W., 1981, A&A, 100, 169
—, 2010, Ap&SS, 329, 151
Hamann W., Gräfener G., 2003, A&A, 410, 993
—, 2004, A&A, 427, 697
Hamann W., Koesterke L., 1998, A&A, 333, 251
Hamann W.-R., Brown J. C., Feldmeier A., Oskinova L. M., 2001, A&A, 378, 946
Henrichs H. F., de Jong J. A., Donati D., Wade G. A., Babel J., Shorlin S. L. S., Verdugo E., Talavera A., Catala C., Veen P. M., Nichols J. S., Kaper L., 2000, in Magnetic Fields of Chemically Peculiar and Related Stars, Y. V. Glagolevskij & I. I. Romanyuk, ed., pp. 57–60
Henrichs H. F., Schnerr R. S., ten Kulve E., 2005, in Astronomical Society of the Pacific Conference Series, Vol. 337, The Nature and Evolution of Disks Around Hot Stars, R. Ignace & K. G. Gayley, ed., p. 114
Hillier D. J., Miller D. L., 1999, ApJ, 519, 354
Hubrig S., Briquet M., Morel T., Schöller M., González J. F., De Cat P., 2008, A&A, 488, 287
Hubrig S., Briquet M., Schöller M., De Cat P., Mathys G., Aerts C., 2006, MNRAS, 369, L61
Hubrig S., Ilyin I., Schöller M., Briquet M., Morel T., De Cat P., 2011, ApJ, 726, L5+
Hunger K., Heber U., Groote D., 1989, A&A, 224, 57
Ignace R., Oskinova L. M., Jardine M., Cassinelli J. P., Cohen D. H., Donati J., Townsend R. H. D., ud-Doula A., 2010, ApJ, 721, 1412
Kaper L., Henrichs H. F., Fullerton A. W., Ando H., Bjorkman K. S., Gies D. R., Hirata R., Kambe E., McDavid D., Nichols J. S., 1997, A&A, 327, 281
Krtička J., Kubát J., 2000, A&A, 359, 983
Leone F., 1994, A&A, 286, 486
Li Q., Cassinelli J. P., Brown J. C., Waldron W. L., Miller N. A., 2008, ApJ, 672, 1174
Liermann A., Hamann W., Oskinova L. M., Todt H., Butler K., 2010, A&A, 524, A82
Lucy L. B., 2010, A&A, 512, A33
Lucy L. B., Solomon P. M., 1970, ApJ, 159, 879
Macfarlane J. J., Cassinelli J. P., 1989, ApJ, 347, 1090
Maheswaran M., 2003, ApJ, 592, 1156
Maheswaran M., Cassinelli J. P., 2009, MNRAS, 394, 415
Marcolino W. L. F., Bouret J., Martins F., Hillier D. J., Lanz T., Escolano C., 2009, A&A, 498, 837
Martins F., Schaerer D., Hillier D. J., Meynadier F., Heydari-Malayeri M., Walborn N. R., 2005, A&A, 441, 735
Mewe R., Raassen A. J. J., Cassinelli J. P., van der Hucht K. A., Miller N. A., Güdel M., 2003, A&A, 398, 203
Morel M., Magnenat P., 1978, A&AS, 34, 477
Morel T., Butler K., 2008, A&A, 487, 307
Morel T., Hubrig S., Briquet M., 2008, A&A, 481, 453
Mullan D. J., 2009, ApJ, 702, 759
Nazé Y., 2009, A&A, 506, 1055
Nazé Y., Ud-Doula A., Spano M., Rauw G., De Becker M., Walborn N. R., 2010, A&A, 520, A59+
Neiner C., Geers V. C., Henrichs H. F., Floquet M., Frémat Y., Hubert A., Preuss O., Wiersema K., 2003a, A&A, 406, 1019
Neiner C., Henrichs H. F., Floquet M., Frémat Y., Preuss O., Hubert A., Geers V. C., Tijani A. H., Nichols J. S., Jankov S., 2003b, A&A, 411, 565
Oskinova L. M., Hamann W., Feldmeier A., 2007, A&A, 476, 1331
Owocki S. P., Puls J., 2002, ApJ, 568, 965
Petit V., Massa D. L., Marcolino W. L. F., Wade G. A., Ignace R., 2011, MNRAS, L196+
Petit V., Wade G. A., Drissen L., Montmerle T., Alecian E., 2008, MNRAS, 387, L23
Prinja R. K., 1989, MNRAS, 241, 721
Raassen A. J. J., Cassinelli J. P., Miller N. A., Mewe R., Tepedelenlioğlu E., 2005, A&A, 437, 599
Reiners A., Stahl O., Wolf B., Kaufer A., Rivinius T., 2000, A&A, 363, 585
Remage Evans N., DeGioia-Eastwood K., Gagné M., Townsley L., Broos P., Wolk S., Nazé Y., Corcoran M., Oskinova L., Moffat A. F. J., Wang J., Walborn N. R., 2011, ApJS, 194, 13
Robrade J., Schmitt J. H. M. M., 2011, ArXiv e-prints
Rogerson Jr. J. B., Upson II W. L., 1977, ApJS, 35, 37
Romanyuk I. I., Kudryavtsev D. O., 2008, Astrophysical Bulletin, 63, 139
Sanz-Forcada J., Franciosini E., Pallavicini R., 2004, A&A, 421, 715
Schnerr R. S., Henrichs H. F., Neiner C., Verdugo E., de Jong J., Geers V. C., Wiersema K., van Dalen B., Tijani A., Plaggenborg B., Rygl K. L. J., 2008, A&A, 483, 857
Schnerr R. S., Henrichs H. F., Oudmaijer R. D., Telting J. H., 2006, A&A, 459, L21
Silvester J., Neiner C., Henrichs H. F., Wade G. A., Petit V., Alecian E., Huat A., Martayan C., Power J., Thizy O., 2009, MNRAS, 398, 1505
Simón-Díaz S., García-Rojas J., Esteban C., Stasińska G., López-Sánchez A. R., Morisset C., 2011, A&A, 530, A57+
Skrutskie M. F., Cutri R. M., Stiening R., Weinberg M. D., Schneider S., Carpenter J. M., Beichman C., Capps R., Chester T., Elias J., Huchra J., Liebert J., Lonsdale C., Monet D. G., Price S., Seitzer P., Jarrett T., Kirkpatrick J. D., Gizis J. E., Howard E., Evans T., Fowler J., Fullmer L., Hurt R., Light R., Kopan E. L., Marsh K. A., McCallon H. L., Tam R., Van Dyk S., Wheelock S., 2006, AJ, 131, 1163
Sota A., Maíz Apellániz J., Walborn N. R., Alfaro E. J., Barbá R. H., Morrell N. I., Gamen R. C., Arias J. I., 2011, ApJS, 193, 24
Springmann U. W. E., Pauldrach A. W. A., 1992, A&A, 262, 515
Stankov A., Handler G., 2005, ApJS, 158, 193
Strüder L., Briel U., Dennerl K., Hartmann R., Kendziorra E., Meidinger N., Pfeffermann E., Reppin C., Aschenbach B., Bornemann W., Bräuninger H., Burkert W., Elender M., Freyberg M., Haberl F., Hartner G., Heuschmann F., Hippmann H., Kastelic E., Kemmer S., Kettenring G., Kink W., Krause N., Müller S., Oppitz A., Pietsch W., Popp M., Predehl P., Read

A., Stephan K. H., Stötter D., Trümper J., Holl P., Kemmer J., Soltau H., Stötter R., Weber U., Weichert U., von Zanthier C., Carathanassis D., Lutz G., Richter R. H., Solc P., Böttcher H., Kuster M., Staubert R., Abbey A., Holland A., Turner M., Balasini M., Bignami G. F., La Palombara N., Villa G., Buttler W., Gianini F., Lainé R., Lumb D., Dhez P., 2001, A&A, 365, L18
Sutherland R. S., Dopita M. A., 1993, ApJS, 88, 253
Suzuki T. K., Yan H., Lazarian A., Cassinelli J. P., 2006, ApJ, 640, 1005
Telting J. H., Aerts C., Mathias P., 1997, A&A, 322, 493
Todt H., Peña M., Hamann W., Gräfener G., 2010, A&A, 515, A83
Townsend R. H. D., Owocki S. P., Ud-Doula A., 2007, MNRAS, 382, 139
Turner M. J. L., Abbey A., Arnaud M., Balasini M., Barbera M., Belsole E., Bennie P. J., Bernard J. P., Bignami G. F., Boer M., Briel U., Butler I., Cara C., Chabaud C., Cole R., Collura A., Conte M., Cros A., Denby M., Dhez P., Di Coco G., Dowson J., Ferrando P., Ghizzardi S., Gianotti F., Goodall C. V., Gretton L., Griffiths R. G., Hainaut O., Hochedez J. F., Holland A. D., Jourdain E., Kendziorra E., Lagostina A., Laine R., La Palombara N., Lortholary M., Lumb D., Marty P., Molendi S., Pigot C., Poindron E., Pounds K. A., Reeves J. N., Reppin C., Rothenflug R., Salvetat P., Sauvageot J. L., Schmitt D., Sembay S., Short A. D. T., Spragg J., Stephen J., Strüder L., Tiengo A., Trifoglio M., Trümper J., Vercellone S., Vigroux L., Villa G., Ward M. J., Whitehead S., Zonca E., 2001, A&A, 365, L27
ud-Doula A., Owocki S. P., 2002, ApJ, 576, 413
van Leeuwen F., 2007, A&A, 474, 653
Vink J. S., de Koter A., Lamers H. J. G. L. M., 2000, A&A, 362, 295
Votruba V., Feldmeier A., Kubát J., Rätzel D., 2007, A&A, 474, 549
Walborn N. R., Fitzpatrick E. L., 1990, PASP, 102, 379
Weidner C., Vink J. S., 2010, A&A, 524, A98
Yudin R. V., 2001, A&A, 368, 912
Zhekov S. A., Palla F., 2007, MNRAS, 382, 1124